Title
Investigating Regulators of Daughter Cell Size Asymmetry in the C. elegans Q Neuroblast Lineage

Author
Robinson, Joseph Dehoney

Publication Date
2022

Peer reviewed|Thesis/dissertation

Investigating Regulators of Daughter Cell Size Asymmetry in the *C. elegans* Q Neuroblast Lineage

By

Joseph Dehoney Robinson

A dissertation submitted in partial satisfaction of the

requirements for the degree of

Doctor of Philosophy

in

Molecular and Cell Biology

in the

Graduate Division

of the

University of California, Berkeley

Committee in Charge:

Professor Gian Garriga, Chair
Professor David Bilder
Professor Michael Shapira
Professor David Weisblat

Fall 2022

Abstract

Investigating Regulators of Daughter Cell Size Asymmetry in the
C. elegans Q Neuroblast Lineage

By

Joseph Dehoney Robinson

Doctor of Philosophy in Molecular and Cell Biology

University of California, Berkeley

Professor Gian Garriga, Chair

Asymmetric cell division (ACD) is an important mechanism that generates cellular diversity during development. Not only do asymmetric cell divisions produce daughter cells of different fates, many can produce daughters of different sizes, which we refer to as Daughter Cell Size Asymmetry (DCSA). In *C. elegans,* apoptotic cells are frequently produced by asymmetric divisions that exhibit DCSA, where the smaller daughter dies. We focus here on the divisions of the Q.a and Q.p neuroblasts, which produce apoptotic cells and divide with opposite polarity using both distinct and overlapping mechanisms.

The PIG-1/MELK and TOE-2 proteins both regulate DCSA and specify the apoptotic cell fate in both the Q.a and Q.p divisions. In many asymmetric cell divisions, the non-muscle myosin NMY-2 is involved in properly positioning the cleavage furrow to produce daughters of unequal size. It was previously reported that NMY-2 is asymmetrically distributed and required for the DCSA of Q.a but not Q.p. In this study, we examined endogenously tagged reporters of NMY-2, TOE-2, and PIG-1 and found that all were asymmetric at the cortex during both the Q.a and Q.p divisions. TOE-2 and NMY-2 were biased toward the side of the dividing cell that would produce the smaller daughter, whereas PIG-1 was biased toward the side that would produce the larger daughter. We used temperature-sensitive *nmy-2* mutants to determine the role of *nmy-2* in these divisions and found that these mutants only displayed DCSA defects in the Q.p division. We generated double mutant combinations between the *nmy-2* mutations and mutations in *toe-2* and *pig-1.* The *nmy-2* mutations did not significantly alter the DCSA of the *toe-2* and *pig-1* mutants but did alter the fate of the Q.a and Q.p daughters. This finding suggests that NMY-2 functions together with TOE-2 and PIG-1 to regulate DCSA but plays an independent role in specifying the fate of the Q.a and Q.p descendants.

This dissertation is dedicated to my family

Table of Contents

Acknowledgments

I would like to first thank the faculty of the Gettysburg College Biology Department for their help and early support of my work, and particularly. Dr. Jennifer Powell, who was my PI for my entire undergraduate career. My time in the Powell Lab taught me that I do, in fact, love research, despite how frustrating it may frequently be. It also taught me that sometimes the weirdest, most inexplicable results can lead to novel discoveries. In her lab I learned how to work with C. elegans, how to perform genetic analysis, how to read and understand scientific papers, and how to design and perform experiments. I cannot overstate her importance in getting me where I am today. Thank you so much.

At UC Berkeley, I must first thank Gian Garriga. His help, support, understanding, and patience are what allowed me to graduate despite all the challenges faced. I also would like to thank Richard Ikegami for his guidance as I acclimated to the new lab, for being an excellent person to talk to, and for being a great troubleshooter. While technically not a current member of the Garriga Lab, Jérôme Teulière also provided invaluable training and guidance from afar, helping me with protocols, methods and analysis.

I would also like to thank the other faculty at Berkeley who helped me on my journey to this point. My thesis committee: David Bilder, David Weisblatt, and Michael Shapira, who have provided insight and advice throughout my time in the Garriga lab. I must also thank Matt Welch, because without his support and guidance I may well have dropped out of the program. Thank you for letting me temporarily be a member of your lab.

Thank you to the Meyer lab, especially Nick Fuda and Behnom Farboud, for their assistance and training with C. elegans injections and gene editing, as well as general troubleshooting assistance. I also would like to thank the members of the Dernburg lab for their help and support. Particularly Weston Stauffer and Chenshu Liu – thank you for providing me with the microscope and the training I needed to perform my time-lapse imaging experiments.

I also must thank my friends for keeping me sane throughout this process. Their support kept me going in my roughest times. Ceci and Emily in particular have helped me more than I could possibly repay. Special thanks to Ceci for encouraging me for over a decade of me pulling my hair out over science they did not understand. And my partner Kat. There is no-one else I would rather have been locked in with for an entire pandemic, and you've made these last four years a joy.

Finally, nothing I've done would be possible without my family. No one has been more supportive of my time here while simultaneously wanting it to end as soon as possible. Love you Mom and Jenna!

Chapter 1: Introduction

1.1 Asymmetric Cell Division

Metazoan development begins with a single cell. That cell gives rise to all the diverse cell types, tissues and organs that compose the adult organism. One process that can contribute to the generation of diverse cell types is Asymmetric Cell Division (ACD), where a single cell divides to produce daughters that exhibit different cell fates. The differing daughter cell fates can be determined by both cell-intrinsic and cell-extrinsic mechanisms. Extrinsic mechanisms involve signaling from surrounding cells or between daughter cells to polarize the dividing cell and generate two daughters with distinct fates or to make two initially identical cells adopt different cell fates. Intrinsic mechanisms involve molecules that are asymmetrically distributed in the progenitor cell and specify the fate of the daughter cell that inherit them. Both intrinsic and extrinsic mechanisms can contribute to ACD.

Well-known examples of extrinsic mechanisms include the Notch and Wnt signaling pathways. In Notch signaling, the Notch ligand is a transmembrane protein expressed on the surface of a signaling cell, which can be a neighboring cell or one of the two daughter cells. The ligand binds to Notch receptors on the surface of neighboring or sister cell to specify the fate of the receiving cell (for recent reviews see (Kopan, 2012; Schweisguth, 2015)). Wnts, secreted glycoproteins, also regulate ACD. Wnts can polarize the progenitor cell, the receiving cells inheriting different fates depending on the local concentration of Wnt ligand (for a review see (Lam & Phillips, 2017)

My focus in this chapter is on intrinsic ACD. A generalized mechanism of intrinsic ACD is the asymmetric distribution of cell-fate determinants resulting in one daughter cell inheriting more or less of a given determinant or set of determinants. I will discuss specific examples of these cell-fate determinants later in this chapter. Crucial to intrinsic asymmetry is that cell polarity must be established, and the mitotic spindle must be oriented accordingly during the division.

In practice, development involves a complex interplay between both intrinsic and extrinsic asymmetries. Both signaling and intrinsic asymmetries can contribute to ACD. For example, in *Drosophila melanogaster* neuroblast development, the basal daughter cells inherits Notch signaling inhibitor Numb, such that their responses to the Notch signal are distinct. The asymmetric response to the signal permits the differentiation of the basal cell, while the apical cell continues to be a proliferating neuroblast (for review see (Gallaud et al., 2017).

Another mechanism of intrinsic ACD is Daughter Cell Size Asymmetry (DCSA), which results in daughter cells of unequal size and fate, requiring not just polarity establishment and spindle orientation, but also an asymmetric cleavage furrow (Horvitz & Herskowitz, 1992). The purpose of the size asymmetry is largely unknown, though recent work in the *C. elegans* first cell division has demonstrated that it is required for robust development (Jankele et al., 2021). I will focus on a review of DCSA in this chapter.

1.2 DCSA in the C. elegans First Cell Division

C. elegans is a particularly useful model system for studying ACD as its lineage is invariant. One of the most well-studied examples of ACD and DCSA is the division of the *Caenorhabditis elegans* zygote. In the first division, the zygote divides into a larger anterior and smaller posterior cell. After fertilization, the sperm nucleus and centrosome enter the cell and initiate a signaling cascade that causes the asymmetric redistribution of several previously symmetrical components. This polarization is maintained throughout the first division, and the asymmetrically localized proteins regulate the posterior positioning of the spindle and cleavage furrow (Fig 1.1) (Pacquelet, 2017).

Before polarization, a complex of PAR-3 (Drosophila: baz, Mammal: Pard3), PAR-6 (Drosophila: par-6, Mammal: Pard6), and PKC-3 (Drosophila: aPKC, Mammal: Prkci/z) localizes uniformly to the cell cortex (Fig 1.1). PAR-1 (Drosophila: par-1, Mammal: Mark2) and PAR-2 (non-conserved) are likely and known, respectively, targets of PKC-3 phosphorylation. This phosphorylation prevents their localization to the cortex (Zonies et al., 2010). After fertilization, a proximity-dependent but currently unknown signal from the sperm centrosome results in the removal of the RHO GEF ECT-2 from the cortex on the posterior of the cell (Fig 1.1) (Cowan & Cowan, 2004; Hird & White, 1993; Munro et al., 2004; Sadler & Shakes, 2000). The lack of ECT-2 leads to the inactivation of the non-muscle myosin, NMY-2, in that region, resulting in movement of the actomyosin network and cortical flow towards the anterior (Zonies et al., 2010). This anterior flow localizes the PAR-3/PAR-6/PKC-3 PAR complex to the anterior cortex (Fig 1.1). In the absence of PKC-3, PAR-1 and PAR-2 localize to the cortex on the posterior of the cell (Fig 1.1). These proteins in turn regulate the positioning of the various components required for the other aspects of asymmetric cell division.

Spindle positioning is one of the key aspects of asymmetric cell division. In the first mitotic division, the Gα/GPR/LIN-5 complex acts as an anchor between the cell cortex and astral microtubule-associated dynein (Couwenbergs et al., 2007; Galli et al., 2011; Gotta et al., 2003; Nguyen-Ngoc et al., 2007; Park & Rose, 2008). The two Gα subunits, GOA-1 and GPA-16, are held in their GDP bound form by binding to the G protein regulators GPR-1 and GPR-2, the *C. elegans* homologs of mammalian LGN. LIN-5, the *C. elegans* homolog of mammalian NuMA, binds to GPR-1/2 and connects this complex to a dynein complex including DYRB-1, DHC-1, and LIS-1 (Couwenbergs et al., 2007; Nguyen-Ngoc et al., 2007). In *C. elegans*, it is likely that the interaction of GRP-1/2 with GOA-1/GPA-16 is dependent on LIN-5, as depletion or loss of LIN-5 results in loss of GPR-1/2 cortical localization (Gotta et al., 2003). Interestingly, in the absence of GPR-1/2 there is still LIN-5 at the cortex, though it is reduced, suggesting the presence of a GRP-1/2 independent mechanism for targeting LIN-5 to the cortex (Park & Rose, 2008).

The localization of the Gα/GPR/LIN-5 complex is crucial to its function. The complex localizes to the posterior pole of the embryo during the first mitotic division, increasing the pulling forces on the spindle at the posterior (Fig 1.1) (Krueger et al., 2010). The Gα/GPR/LIN-5 complex is prevented from localizing to the anterior by the action of the PAR complex, via PKC-3 phosphorylation of LIN-5 (Galli et al., 2011). The Gα/GPR/LIN-5 complex is further focused at

the posterior by LET-99, a DEP-containing protein that localizes to a circumferential band of cell cortex centered on the spindle midpoint, just to the posterior of the embryo midpoint (Fig 1.1). LET-99 inhibits the Gα/GPR/LIN-5 complex from associating with the cortex, reducing lateral pulling forces and further increasing the posterior directed pulling forces (Krueger et al., 2010). The regulation of LET-99 localization is still under investigation. LET-99 is excluded from the anterior and posterior of the embryo by the Core Polarity Complex and the combination of PAR-1 and PAR-5, respectively (Wu et al., 2016; Wu & Rose, 2007). At the posterior, LET-99 is phosphorylated by PAR-1, which permits the binding of the 14-3-3 protein PAR-5 to the 14-3-3 binding sites on LET-99, preventing the association of LET-99 with the posterior cortex. The mechanism preventing phosphorylated LET-99 from associating to the anterior cortex is currently unknown, though it appears to involve phosphorylation by PKC-3. (Wu et al., 2016; Wu & Rose, 2007).

Cleavage furrow positioning is regulated by spindle-dependent and independent mechanisms. Many experiments have been performed that involve shifting the furrow through chemical, genetic, and physical manipulations. In experiments where the spindle is shifted to the posterior by chemical or genetic disruption of the cytoskeleton, two spatially and temporally separated furrows temporarily form, the first between the asters, the second at the spindle midzone. (Bringmann & Hyman, 2005; Werner et al., 2007).

Spindle midzone signaling is dependent on ZEN-4 and CYK-4, the centralspindilin complex. ZEN-4 is a kinesin-like protein that localizes to the spindle midbody and is required for its function (Raich et al., 1998). CYK-4 is a RhoGAP that localizes to the plasma membrane, the spindle midbody and the ring channels in the rachis of the germline (Jantsch-Plunger et al., 2000). The two form a complex, *in vivo* and *in vitro*. This centralspindilin complex is sufficient to induce microtubule bundling *in vitro* (Mishima et al., 2002). Centralspindilin is required for robust organization of the midbody and contractile ring, and its localization is regulated via Cdk1 phosphorylation of ZEN-4 (Mishima et al., 2004). It is hypothesized that CYK-4 interacts with ECT-2 to recruit Rho and Rho effectors, including the nonmuscle myosin NMY-2 to the cleavage furrow (Basant & Glotzer, 2017).

A centralspindlin-independent, though potentially aster-dependent, mechanism of cleavage furrow positioning involves the regulation of cortical actomyosin and Rho effectors. This relies on some of the spindle positioning machinery previously discussed: these include Gα/GPR-1/2 and LET-99; the actomyosin pathway components RhoA, ECT-2, NMY-2 and ANI-1, an Anillin; and NOP-1 a nematode specific protein with no recognizable domains or motifs (Bringmann et al., 2007; Dechant & Glotzer, 2003; Pacquelet et al., 2015; Tse et al., 2012). These components and their roles were determined by experiments where where the spindle midzone, and therefore centralspindlin, is shifted to produce two spatially and temporally separated furrows, or centralspindilin signaling is eliminated either via ablation of the spindle midzone or mutation of centralspindlin components (Bringmann et al., 2007; Tse et al., 2012).

The requirement for Gα/GPR-1/2 and LET-99 is hypothesized to arise from their role in spindle elongation, positioning the spindles and asters towards the posterior via the previously

discussed pulling forces (Bringmann et al., 2007; Dechant & Glotzer, 2003). In worms where LET-99 has been depleted, GPR-1/2 accumulate at the location that would otherwise become the furrow, leading to mis-localization of the asters and the suppression of actomyosin in that region, thereby preventing furrow ingression (Bringmann et al., 2007). The astral microtubules themselves appear to regulate furrowing by preventing myosin accumulation where they contact the cortex, as demonstrated by experiments that show myosin accumulation throughout the cortex when spindle asters have been lost or GPR-1/2 have been depleted (Tse et al., 2011; Werner et al., 2007). The mechanism of this inhibition appears to be that NMY-2 is removed from the cortex in a dynein-mediated transport process (Chapa-Y-Lazo et al., 2020). If this removal of NMY-2 does not occur, the cleavage furrow is shifted towards the anterior. This removal of NMY-2 can also be inhibited by increasing the activity of RhoA, via either depletion of the RhoGAPs RGA-3/4 or gain-of-function mutation of *ect-2* RhoGEF.

The aster-mediated inhibition of NMY-2 also requires ANI-1, one of the two Anillins in *C. elegans*. Anillin is a conserved scaffolding protein connecting F-Actin, non-muscle Myosin II, RhoA, Microtubules and Septins (Piekny & Glotzer, 2008; Tse et al., 2012). During anaphase, ANI-1 localizes to the contractile ring. A proposed mechanism for this localization, derived from work in mammalian cells, is that RhoA-GTP binds to anillin, exposing the NLS, which then can bind to importin-β (Beaudet et al., 2017). During mitosis, there is an inverse correlation between Ran activity and importin levels, resulting in higher levels of importin near the cortex (Beaudet et al., 2017). This results in Anillin localizing to the cortex in a RhoA-GTP and Ran-dependent manner (Beaudet et al., 2017). In *C. elegans,* NOP-1 regulates RhoA activity via ECT-2, which in turn regulates ANI-1 localization, though the mechanism is otherwise unknown (Tse et al., 2012).

ANI-1 plays a role in removing NMY-2 from the anterior cortex during Anaphase and concentrating it at the contractile ring, possibly by mediating the interaction with the astral microtubules and the subsequent dynein-mediated removal of both ANI-1 and NMY-2 (Chapa-Y-Lazo et al., 2020). The removal of NMY-2 from the anterior cortex is also regulated by a parallel pathway involving PAR-4's regulation of PIG-1 MELK kinase, though the precise mechanism for this regulation has yet to be fully established (Pacquelet et al., 2015). ANI-1 is inhibited by ANI-2, which lacks the putative myosin and actin-binding domains of ANI-1, and is presumed to inhibit ANI-1 via competitive binding (Goupil et al., 2017). ANI-2 is suppressed by PAR-4 and the cullin CUL-5 (Pacquelet et al., 2015).

Genetically, aster-dependent furrow positioning requires Gα/GPR-1/2, ANI-1 and NOP-1. For Gα/GPR-1/2, this requirement is hypothesized to be connected to their role in spindle elongation, positioning the spindles and asters towards the posterior via the previously discussed pulling forces (Bringmann et al., 2007; Dechant & Glotzer, 2003). The aster microtubules also appear to regulate furrowing by preventing myosin accumulation where they contact the cortex, as demonstrated by experiments that show myosin accumulation throughout the cortex when spindle asters have been lost or GPR-1/2 have been depleted (Tse et al., 2011; Werner et al., 2007). Also, mispositioning the spindle results in reduction of cortical

myosin near the spindle asters and the formation of a furrow aligned with the spindle midzone, regardless of the orientation of the spindle (Basant et al., 2015).

1.3 DCSA in *C. elegans* Neuroblasts: HSN

An early study demonstrating the contribution of DCSA to neuroblast fate was a screen for genes that cause defects in the development and migrations of the Hermaphrodite Specific Neurons (HSNs), serotonergic motor neurons that innervate the vulval muscles and regulate egg laying (Desai et al., 1988). This screen of egg-laying defective mutants identified a genetic pathway that regulates the development and function of the HSN. Near the top of this pathway is the gene *ham-1*, the loss of which results in both migration-defective and extra HSN neurons (Desai et al., 1988). Subsequent experiments showed that the HAM-1 protein accumulates on the side of the HSN/PHB neuroblast that will produce the posterior daughter cell, the HSN/PHB precursor, while the anterior daughter cell inherits low levels of HAM-1 and dies (Guenther & Garriga, 1996). A following study showed that this division is asymmetric in size as well as in fate with the smaller cell adopting the apoptotic fate. Loss of HAM-1 reverses the asymmetry of the division to generate larger anterior and smaller posterior daughter cells (Frank et al., 2005).

An analysis of the divisions affected by the *ham-1* mutations revealed that *ham-1* loss primarily affects divisions that produce smaller anterior and larger posterior daughter cells, either reversing the divisions or making them more symmetric (Teuliere et al., 2018). This study also revealed that *ham-1* loss affects DCSA asymmetry in divisions that normally produced two daughter cells that survive. Thus, the role of HAM-1 is primarily in ensuring DCSA and its effect on apoptosis is indirect. Further characterization of the HAM-1 protein identified it as the ortholog of human Storkhead box 1 (STOX1), a known transcription factor (Feng et al., 2013; Leung et al., 2016). Additionally, it was found that HAM-1::GFP could be detected in the nucleus, however, the same HAM-1::GFP could not be detected in the nucleus via antibody staining for HAM-1 or GFP (Leung et al., 2016). HAM::GFP also localized asymmetrically to the cortex in several asymmetric divisions (Leung et al., 2016; Teuliere & Garriga, 2018). Both nuclear and cortical localization are necessary for its function in different lineages (Frank et al., 2005; Leung et al., 2016; Teuliere & Garriga, 2018).

1.4 DCSA in *C. elegans* Neuroblasts: NSM

The NSM neuroblast lineage exhibits DCSA mediated programmed cell death. During embryonic development, the NSM neuroblast (NSMnb) divides asymmetrically and gives rise to a larger daughter, the NSM, which differentiates into a serotonergic motor neuron, and a smaller daughter, the NSM sister cell (NSMsc), which dies shortly after the division (Sulston et al., 1983).

One key regulator of this function is PIG-1/MELK, the absence of which reduces asymmetry and a slightly increases the frequency of NSMsc survival (Wei et al., 2017). The authors propose that PIG-1/MELK dependent phosphorylation removes NMY-2 from the dorsal side of the NSMnb, which will produce the cell that dies. Whether this is a direct or indirect phosphorylation is

unknown. PIG-1 appears to function downstream of the conserved complex of PAR-4/LKB1, STRD-1/STRAD and MOP-25.1/2/MO25. NMY-2 localization to the ventral side of the NSM neuroblast following its removal from the dorsal side results in a hypothesized increased membrane contractility and cortical flows towards that side (Fig 1.2) (Wei et al., 2020). This results in shifting the cleavage furrow dorsally. The cortical flows also cause CES-1, a Snail-like transcription factor and ortholog of Drosophila scrt and mammalian Scrt1/2, to localize towards the ventral side of the NSM (Fig 1.2). The cell therefore divides asymmetrically such that the ventral side is larger and has a higher concentration of CES-1 (Fig 1.2) (Wei et al., 2020). The higher concentration of CES-1 in turn leads to the ventral daughter's survival as CES-1 suppresses the transcription of canonical apoptosis pathway protein *egl-1* BH3-only (Wei et al., 2020).

In parallel to the regulation of CES-1, the activity of the caspase CED-3 is also asymmetric (Fig 1.2) (Chakraborty et al., 2015). Using a reporter based on a centriolar protein, TAC-1, that has a caspase cleavage site, the authors generated a TAC-1 separated from GFP by a CED-3 cleavage site, allowing them to monitor relative caspase activity at the two centrosomes. They observed that there are asymmetric levels of caspase activity at the centrioles of the dorsal and ventral sides of the NSMnb, with more activity on the dorsal side of the NSMnb that generates the daughter fated to die (Chakraborty et al., 2015). This finding suggests that there is a gradient of caspase activity between the dorsal and ventral sides of the NSMnb, which is supported by loss of the asymmetry in *ced-3* mutants (Fig 1.2). The caspase activity also required the canonical upstream components of the cell death pathway EGL-1 BH3-only, CED-9 Bcl-2, and CED-4 Apaf-1 (Chakraborty et al., 2015). The loss of this asymmetry correlated with an increase in NSMsc survival.

Together, these provide clear examples of, and potential mechanisms by which, the asymmetry of the division directly controls apoptotic cell fate via sequestration of pro and anti-apoptotic factors.

1.5 DCSA in *Drosophila* Neuroblasts

Many of the components required for asymmetric cell division in *C. elegans* have been implicated in DCSA in other species. *Drosophila* neuroblasts divide asymmetrically producing a self-renewing neuroblast stem cell and a ganglion mother cell that will then divide to produce glia, neurons or both (Gallaud et al., 2017). Unlike the first cell division in *C. elegans* there is no symmetry breaking step as the neuroblasts are intrinsically polarized, the apical/basal polarity inherited from an earlier division (Gallaud et al., 2017). This intrinsic polarization, though not fully understood, results in the formation of an Apical Core Polarity complex containing the *Drosophila* homologs of PAR-3 (Bazooka), PAR-6 (Par-6), and PKC-3 (aPKC). As the neuroblasts delaminate from the epithelium, they inherit this Par complex.

During metaphase the apical core polarity complex recruits Inscuteable (Insc) which recruits Gα, Pins and Mud, the Drosophila homologs of the *C. elegans* Gα, LIN-5 and GPR-1/2, respectively (Gallaud et al., 2017; Tsankova et al., 2017). This complex extends the spindle on the apical side

of the cell, resulting in an asymmetrically sized spindle (Fig 1.3). This contrasts with the first *C. elegans* division, in which the Gα/LIN-5/GPR-1/2 complex is localized to the posterior, opposite of the Core Polarity complex of PAR-3/PAR-6/PKC-3, and increases posterior pulling forces, resulting in an asymmetrically positioned spindle (Gotta et al., 2003). Simultaneously different and similar to the mechanism in *C. elegans* is that during late anaphase-telophase, Mud localizes to a crescent on the basal side of the neuroblast, while Pins is not, suggesting that, as in the *C. elegans* zygote there is a Pins independent mechanism for cortical localization of Mud (Siller et al., 2006).

It has also been determined that, as in *C. elegans,* there is a spindle-independent mechanism involving myosin localization that regulates cleavage furrow positioning; however, the regulatory components have not been elucidated to the extent that they have been in *C. elegans*. Three furrow proteins, Anillin, Myosin and Pavarotti, the *C. elegans* ZEN-4 homolog, localize to the basal side of the neuroblast even when the spindle is rotated orthogonally to the apical/dorsal axis (Cabernard et al., 2010). Also, when the spindle is rotated, a second cleavage furrow forms before the spindle-induced cleavage furrow (Cabernard et al., 2010).

One hypothesized mechanism to explain DCSA in *Drosophila* neuroblasts is asymmetric membrane extension, which is thought to be mediated by myosin polarity (Connell et al., 2011). Initially, there is myosin activity around the entire cortex of the cell (Fig 1.3) (Tsankova et al., 2017). Beginning in prophase, myosin activity is downregulated on the apical side, likely due to inhibition of the Rho Kinase Rok by Protein Kinase N (Pkn) (Tsankova et al., 2017). When Pkn is depleted, the higher myosin activity on the apical side and the furrow is initially mispositioned towards the apical side and then shifts to the basal side during the course of the division. This is similar to the case in the *C. elegans* first cell division where failure to inactivate NMY-2 at the anterior results in the cleavage furrow shifting in that direction (Pacquelet et al., 2015; Zhang & Glotzer, 2015).

1.6 The Q Neuroblast lineage

The Q cell neuroblast lineage is an excellent model for studying DCSA and its role in programmed cell death (Teuliere & Garriga, 2017). There are two Q neuroblasts in each worm, one on the left (QL) and one on the right (QR) (Fig 4). Both Q cells undergo a sequence of three asymmetric divisions, two of which produce cells fated to die and have opposite polarity (Fig 4). Each Q cell divides to produce Q.a and Q.p. Q.a divides to produce a smaller anterior daughter Q.aa, which dies, and a larger posterior daughter Q.ap, which differentiates into the A/PQR oxygen sensing neuron (Fig 4). Q.p divides to produce a smaller posterior daughter Q.pp, which dies, and a larger anterior daughter Q.pa, which divides again to produce the A/PVM mechanosensory neuron and SDQL/R interneuron (Fig 4) (Sulston & Horvitz, 1977).

The Q.a and Q.p DCSA events have opposite polarities and divide asymmetrically using distinct mechanisms. The Q.p division relies on a spindle position-dependent mechanism, in which the spindle is shifted towards the posterior, moving the cleavage furrow in that direction (Ou et al., 2010). This shift leads to a smaller posterior daughter cell that dies. In contrast, the spindle is

not repositioned in the Q.a division. Instead, the asymmetry is dependent on membrane extension on the posterior side of the cell to produce a smaller anterior daughter cell that then dies (Ou et al., 2010). The same study indicated that NMY-2 localizes to the anterior of Q.a and hypothesized that its role is to constrict the anterior side, similar to its hypothesized role in Drosophila neuroblasts (Cabernard et al., 2010; Ou et al., 2010). Recent work has shown that the anterior extension of the Q.p membrane also contributes to its DCSA (Teuliere & Garriga, 2018). Further recent work has shown that F-actin asymmetrically accumulates at the side that will produce the larger daughter cell in both the Q.a and Q.p divisions and this localization is regulated by WNT signaling (Chai et al., 2022).

HAM-1 is a key molecule that establishes Q.a polarity (Teuliere & Garriga, 2018). Loss of *ham-1* results in Q.a switching to Q.p polarity: the spindle shifts posteriorly, and the membrane extends anteriorly in *ham-1* mutant Q.a cells, similar to the pattern observed in wild-type Q.p. The Q.p division is unaffected in *ham-1* mutants. HAM-1 is expressed in Q.a and not Q.p. These findings suggest that Q.p polarity is the "default" polarity and expression of HAM-1 in Q.a reverses its polarity. Surprisingly, NMY-2 asymmetry in Q.a was unaffected in *ham-1* mutants (Teuliere & Garriga, 2018).

Despite these differences, many components are required for both divisions. For instance, both divisions require PIG-1 and TOE-2, as both *pig-1* and *toe-2* mutants have a high rate of extra neurons as well as much more symmetric divisions (Chien et al., 2013; Gurling et al., 2014). Also, both have membrane extensions that contribute to the asymmetry of the divisions (Ou et al., 2010; Teuliere & Garriga, 2018). It was shown that CED-3 is required for the asymmetry of the division, and that there were asymmetric levels of CED-3 caspase activity in QL.p (Mishra et al., 2018). A recent work has also shown the involvement of the wnt signalling pathway, specifically *lin-17*, a Frizzled ortholog, and *apr-1*, an APC ortholog are required for DCSA in the Q lineage (Chai et al., 2022). Recent work in the lab has further characterized Wnt signaling in DCSA in the Q lineage, demonstrating that all five Wnts in and the Frizzleds *mom-5* and *lin-17* are all required for Q.a and Q.p DCSA, and that the Frizzleds act autonomously in the Q lineage (J. Teuliere, personal communication). Investigating the components that are shared between the two divisions is one of the focuses of my research, and I will review what we know about the key players.

1.7 PIG-1

PIG-1 (*par-1*-like gene) is the ortholog of the mammalian "Maternal Embryonic Leucine-zipper Kinase" (MELK) gene and a member of the AMPK family of kinases. In vertebrates, MELK has been shown to play a role in a wide range of cellular processes including cell division, differentiation, death and survival. The role of MELK appears to be highly context dependent as there is evidence in different systems and models showing pro- and anti-apoptotic roles (Ganguly et al., 2015). For instance, MELK is known to be expressed at high levels in proliferating cells during development and in many human cancer cell lines and has a potential role in the cell cycle in Xenopus. It is also known to phosphorylate and increase the activity of pro-apoptotic factors, including ASK1 in mice and p53 in HCT116 colon cancer lines, yet also

appears to down-regulate p53 in glioblastoma and HEK 293T cells (Ganguly et al., 2015). Despite its roles in development and cell death, knockouts of PIG-1 are viable in both *C. elegans* and mice (Cordes et al., 2006; Wang et al., 2014).

Our lab first identified PIG-1's role in *C. elegans* asymmetric cell divisions in a screen for worms defective in the HSN/PHB neuroblast division; further characterization of *pig-1* mutants revealed that they were defective in five other neuroblast divisions, including the Q.a and Q.p divisions (Cordes et al., 2006). Later work demonstrated that PIG-1 has a role in positioning the cleavage furrow in the division of the single-cell embryo, where it acts downstream of PAR-4 and in parallel with anillin (ANI-1) (Pacquelet et al., 2015). Another study showed that PIG-1 plays a role in the division of the EMS blastomere at the 4-cell stage, though in this context it has overlapping functions with PAR-1 and acts downstream of MES-1, a Receptor Tyrosine Kinase, and SRC-1, a *C. elegans* SRC ortholog, while PAR-1 acts downstream of a WNT pathway (Liro et al., 2018).

In multiple asymmetric cell divisions including the Q.a and Q.p divisions, PIG-1 has been shown to function downstream of a PAR-4/LKB1, STRD-1/STRADα, MOP-25.1,2/ MO25α complex, presumably through phosphorylation of PIG-1 by PAR-4 kinase (Chien et al., 2013; Denning et al., 2012; Pacquelet et al., 2015; Wei et al., 2020). A threonine in the activation loop of PIG-1, which is conserved in members of the AMPK family and phosphorylated by LKB and its homologs, is essential for PIG-1 activity (Chien et al., 2013). This threonine is conserved in MELK, but unlike the other members of the AMPK family, MELK can autophosphorylate this threonine independent of LKB1 *in vitro* (Lizcano et al., 2004). It is unclear whether PIG-1 has the ability to autophosphorylate, but genetic studies suggest that PAR-4 is the kinase responsible for PIG-1 activation (Chien et al., 2013; Pacquelet et al., 2015).

1.8 TOE-2

TOE-2 was originally identified by bioinformatics and shown biochemically to be a "Target of Erk" (Arur et al., 2009). RNAi of *toe-2* results in an increase in germline apoptosis. TOE-2 was subsequently found to regulate the asymmetric divisions of both Q.a, and Q.p (Gurling et al., 2014). Specifically, TOE-2 is required for Q.a and Q.p DCSA. Loss of TOE-2 causes a range of phenotypes including cell-fate transformations of Q lineage cells and the smaller daughter cells, Q.aa and Q.pp, surviving at an increased frequency. These are more pronounced in the Q.p division than the Q.a division.

TOE-2 has a DEP domain and multiple MPK docking sites (Arur et al., 2009; Gurling et al., 2014). The Disheveled Egl-10 Pleckstrin (DEP) domain is a protein-protein interaction domain typically found in transducers of cellular signaling near the cortex, particularly G-protein signaling. It also bears significant homology with LET-99, a protein that is involved in other asymmetric divisions, including the first cell division, but is not involved in the Q lineage divisions (M. Gurling, unpublished observations)

1.9 NMY-2 and ECT-2

Non-muscle myosin is a central component of the actomyosin network and is involved in a wide variety of processes. As mentioned earlier, the non-muscle myosin NMY-2 plays a key role in establishing the polarity of the first cell division and the DCSA of the NSM and Q.a and Q.p neuroblasts (Guo & Kemphues, 1996; Ou et al., 2010; Wei et al., 2020). NMY-2 acts downstream of RHO-1, which in turn is activated by the Rho-GEF ECT-2 in the *C. elegans* first cell division (Motegi & Sugimoto, 2006).

An interesting complication in the models for NMY-2's role in DCSA is that in different asymmetric cell divisions, it has different localization patterns with respect to the eventual sizes of the daughter cells. In the Q.a division, NMY-2 localizes to the side that will become the smaller daughter cell fated to die (Ou et al., 2010). This is similar to its pattern in Drosophila neuroblasts (Tsankova et al., 2017). In the NSM, however, NMY-2 localizes to the side that will become the larger surviving daughter cell. This is similar to the *C. elegans* first cell division where it localizes to the larger anterior side (Pacquelet, 2017). Moreover, PIG-1 regulates NMY-2 distribution in these *C. elegans* divisions (Chien et al., 2013; Pacquelet et al., 2015; Wei et al., 2020). However, in Q.p, NMY-2 does not appear to be asymmetric (Ou et al., 2010). Considering that in most of these divisions NMY-2 has been shown to play a role in furrow positioning independent of spindle positioning, the fact that the localization of NMY-2's is different in these asymmetric divisions is puzzling. Investigating the role and regulation of NMY-2 localization is another focus of my research.

1.10 The *C. elegans* Germline

An interesting observation over the course of my research is that there is a significant overlap between DCSA components and germline expression, in many cases the DCSA proteins localize to ring channels. During germline development and during gametogenesis germ cells do not completely cellularize. Instead incomplete cytokinesis leads to a syncytium of germ cells connected by large ring channels that open into the central core of the gonad, called the rachis (Goupil et al., 2017). The ring channels only close when a germ cell matures into a gamete. Many of the components involved in this process have also been identified as part of the furrow positioning pathways in the *C. elegans* first cell division, including ZEN-4, CYK-4, NMY-2, ECT-2 and ANI-1 (Goupil et al., 2017; Jantsch-Plunger et al., 2000; Morita et al., 2005).

The proposed mechanism for this process is that RHO activity, influenced by the RHO::GEF ECT-2, and the centralspindilin complex, recruits anillins to the cytoplasmic bridge, which in turn is then required for the recruitment/maintenance of NMY-2, to the channel (Goupil et al., 2017). There are two anillins in *C. elegans,* ANI-1, which is required for cytokinesis, and ANI-2 which is a truncated version and is required for the maintenance of ring channels. Recruitment of ANI-2 to the ring channels appears to limit the amount of ANI-1 present, possibly preventing the closure. The maintenance of the ring channels also depends on the function of NMY-1 (Coffman et al., 2016). The presence of multiple genes involved in DCSA regulation led us to investigate whether the germline could be used as a proxy for screening for other genes involved in DCSA regulators. An RNAi screen for disruption of the rachis led us to further investigate the role of ECT-2 in the Q neuroblast division.

1.11 Project Goal:

Many mechanisms have been partially elucidated for DCSA in multiple contexts, but there are still several gaps. In particular, the *C. elegans* neuroblasts seem to exhibit a variety of different mechanisms for regulating DCSA, producing divisions with different orientations and axes. For instance, NMY-2 localizes to the side fated to live in the NSM division, while it localizes to the side fated to die in the Q.a division. Also, the localization of several key proteins in the Q lineage divisions have yet to be clearly elucidated. In my research, I used a combination of imaging of endogenously tagged proteins, as well as mutant analysis to further explore the roles of TOE-2, NMY-2 and PIG-1 in the Q lineage division.

1.12 Figures:

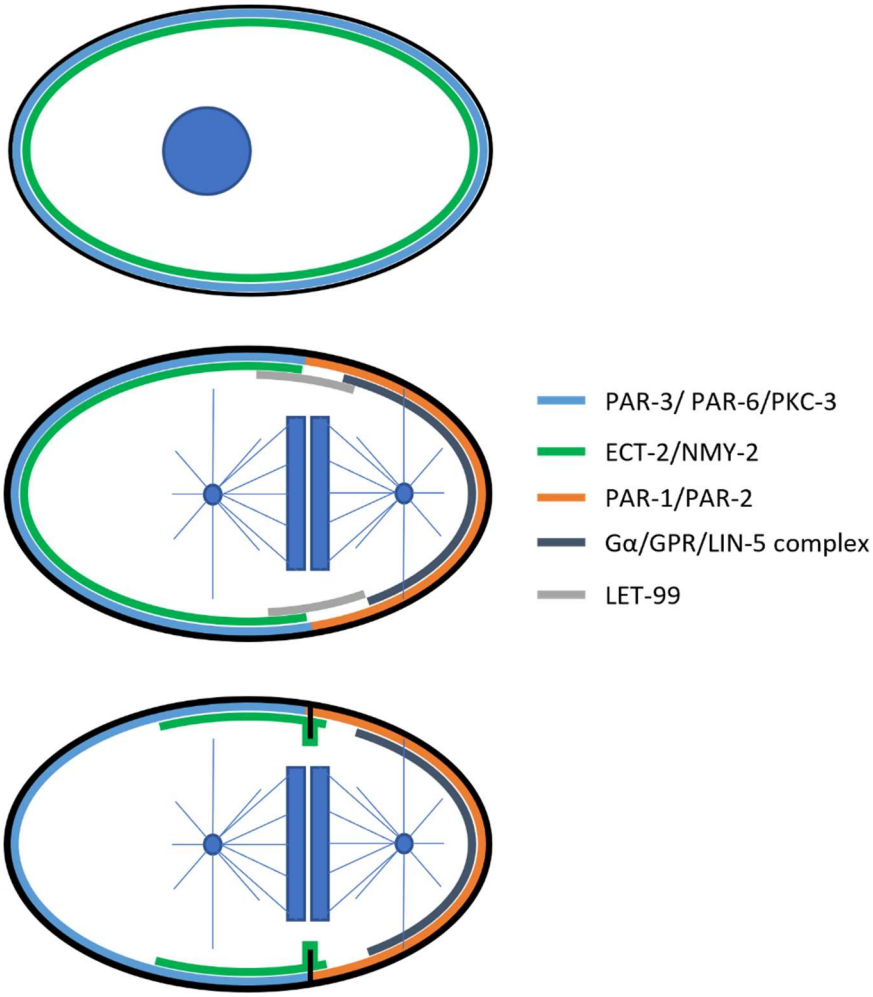

Fig 1.1 DCSA in the C. elegans first cell division.
Key polarity regulators locations are shown in interphase, early metaphase, and late metaphase shortly before anaphase.

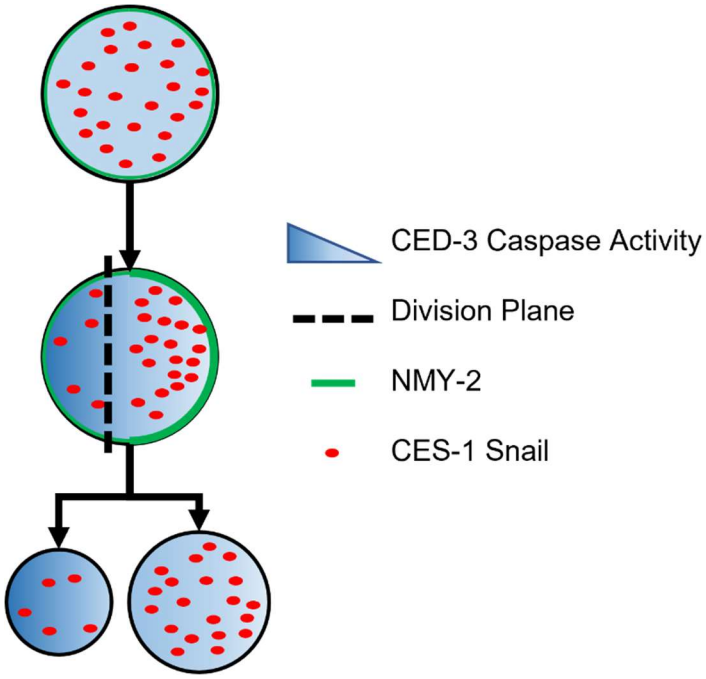

Fig 1.2 DCSA in the *C. elegans* NSM division.
Adapted from (Chakraborty et al., 2015; Wei et al., 2020). The localization of NMY-2 and CES-1 during the NSM neuroblast division are shown along with the hypothesized gradient of CED-3 caspase activity.

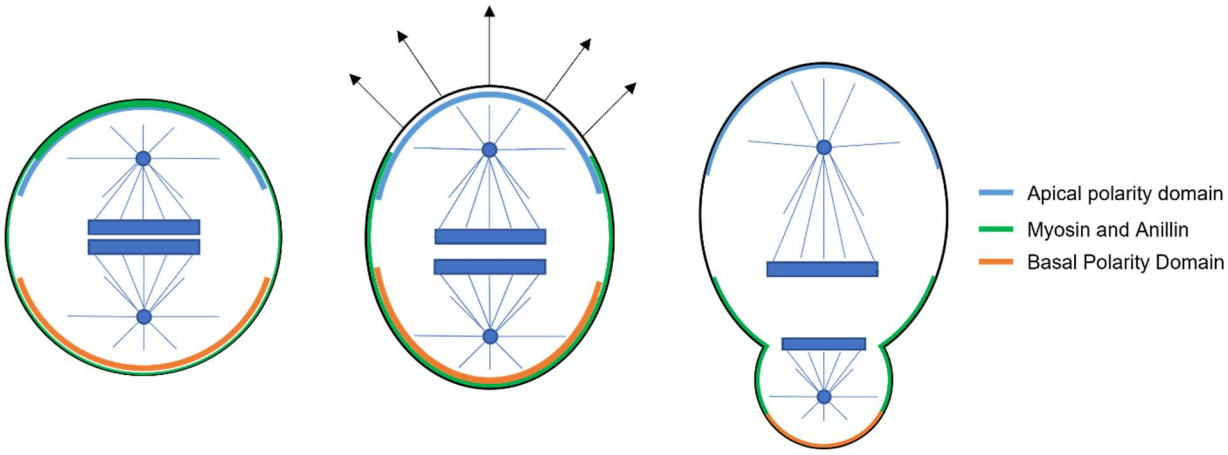

Fig 1.3: Drosophila neuroblast division.
Adapted from (Cabernard et al., 2010; Tsankova et al., 2017). The location of the apical and basal polarity domains as well as the localization of non-muscle myosin and anillin are shown at metaphase, anaphase, and telophase.

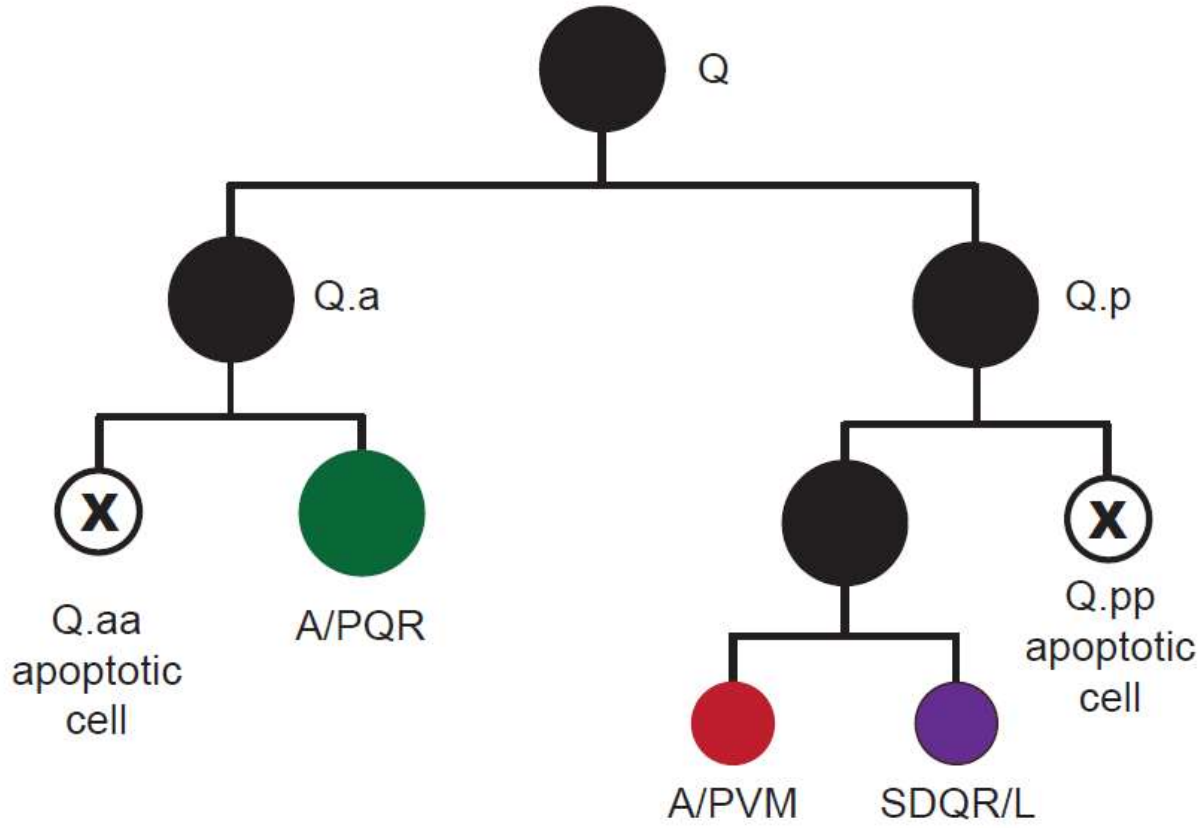

Fig 1.4: Q lineage Division.
Adapted from (Gurling et al., 2014). The Q neuroblast divides to produce Q.a and Q.p, which divide to produce anterior (Q.aa or Q.pa) and posterior (Q.ap or Q.pp) daughter cells. In the Q.a division, the anterior daughter, Q.aa, is smaller and apoptotic. In the Q.p division, the posterior daughter, Q.pp, is smaller and apoptotic.

Chapter 2: NMY-2, TOE-2 and PIG-1 regulate C. elegans asymmetric cell divisions

The following chapter contains material derived from a pre-print publication on which I am first author (Robinson et al., 2022). Some nematode strains used in this work were provided by the Caenorhabditis Genetics Center, which is funded by the NIH Office of Research Infrastructure Programs (P40 OD010440). We also thank Bob Horvitz and Guangshuo Ou for providing some of the strains used in this study. Some of the strains used in this work were constructed in our lab by Jérôme Teulière, Shinja Yoo, and Elena Molitor. Jérôme Teulière also collected some of the DCSA data. We thank Abby Dernburg, Chenshu Liu and Weston Stauffer for the use of their spinning disc confocal microscope and assistance in its use. We thank Nicolas Alexandre for his assistance with statistical analysis.

2.1 Summary

Asymmetric cell division (ACD) is an important mechanism that generates cellular diversity during development. Not only do asymmetric cell divisions produce daughter cells of different fates, many can produce daughters of different sizes, which we refer to as Daughter Cell Size Asymmetry (DCSA). In *C. elegans,* apoptotic cells are frequently produced by asymmetric divisions that exhibit DCSA, where the smaller daughter dies. We focus here on the divisions of the Q.a and Q.p neuroblasts, which produce apoptotic cells and divide with opposite polarity using both distinct and overlapping mechanisms. The PIG-1/MELK and TOE-2 proteins both regulate DCSA and specify the apoptotic cell fate in both the Q.a and Q.p divisions. In many asymmetric cell divisions, the non-muscle myosin NMY-2 is involved in properly positioning the cleavage furrow to produce daughters of unequal size. It was previously reported that NMY-2 is asymmetrically distributed and required for the DCSA of Q.a but not Q.p. In this study, we examined endogenously tagged reporters of NMY-2, TOE-2, and PIG-1 and found that all were asymmetric at the cortex during both the Q.a and Q.p divisions. TOE-2 and NMY-2 were biased toward the side of the dividing cell that would produce the smaller daughter, whereas PIG-1 was biased toward the side that would produce the larger daughter. We used temperature-sensitive *nmy-2* mutants to determine the role of *nmy-2* in these divisions and found that these mutants only displayed DCSA defects in the Q.p division. We generated double mutant combinations between the *nmy-2* mutations and mutations in *toe-2* and *pig-1.* The *nmy-2* mutations did not significantly alter the DCSA of the *toe-2* and *pig-1* mutants but did alter the fate of the Q.a and Q.p daughters. This finding suggests that NMY-2 functions together with TOE-2 and PIG-1 to regulate DCSA but plays an independent role in specifying the fate of the Q.a and Q.p descendants.

2.2 Introduction

A core aspect of development is that a single cell can give rise to multiple cell types. This is often accomplished by ACD, wherein a cell divides to produce daughters with distinct fates. One mechanism contributing to ACD is the asymmetric distribution of cell fate determinants that specify daughter cell fates. Another mechanism contributing to ACD is DCSA, which results in daughter cells of unequal size. Different mechanisms can contribute to a shifted furrow that results in DCSA.

The *C. elegans* Q.a and Q.p neuroblast divisions provide examples of different mechanisms of DCSA (Fig 2.1). These sister cells both divide to produce a smaller daughter cell that dies while exhibiting opposite polarity: Q.a produces the smaller anterior Q.aa daughter, whereas Q.p produces the smaller posterior Q.pp daughter. Mutations that disrupt the size asymmetry also disrupt the apoptotic fate of the smaller daughter cell. Different DCSA mechanisms have been reported for the two cells: Q.a divides by a spindle-independent, HAM-1 and myosin-dependent mechanism, whereas Q.p divides by a spindle-dependent, HAM-1 and myosin-independent mechanism (Feng et al., 2013; Ou et al., 2010; Teuliere & Garriga, 2018). Despite these differences, specific proteins are required for both divisions including the PAR-4/PIG-1 kinase pathway and the DEP-containing protein TOE-2 (Chien et al., 2013; Gurling et al., 2014).

PIG-1 (*par-1*-like gene) is the ortholog of the mammalian Maternal Embryonic Leucine-zipper Kinase (MELK) gene and a member of the AMPK family of kinases. In vertebrates, MELK has been shown to play a role in a wide range of cellular processes, including cell division, differentiation, death, and survival (Ganguly et al., 2015). In *C. elegans*, PIG-1 is involved in numerous asymmetric cell divisions, including the first embryonic division, the NSM neuroblast division, and both the Q.a and Q.p divisions (Cordes et al., 2006; Pacquelet et al., 2015). In several asymmetric cell divisions, PIG-1 has been shown to function downstream of a PAR-4/LKB1, STRD-1/STRADα, MOP-25.1,2/ MO25α complex, presumably through phosphorylation of PIG-1 by PAR-4 kinase (Chien et al., 2013; Denning et al., 2012; Pacquelet et al., 2015; Wei et al., 2020).

TOE-2 was originally identified by bioinformatics and shown biochemically to be a Target of Erk and was subsequently found to regulate both Q.a and Q.p ACD (Arur et al., 2009; Gurling et al., 2014). TOE-2 has a DEP domain and multiple MPK docking sites (Arur et al., 2009; Gurling et al., 2014). The Disheveled Egl-10 Pleckstrin (DEP) domain is a protein-protein interaction domain typically found in transducers of cellular signaling near the cortex, particularly G-protein signaling. Using the predicted structure of TOE-2 from AlphaFold in an NCBI VAST search, we found that TOE-2 also has a region with structural similarity to RhoGAP domains (Gibrat et al., 1996; Jumper et al., 2021; Varadi et al., 2022). The structure of TOE-2 is similar to that of LET-99, a protein that also contains both a DEP domain and a degenerate RhoGAP-like domain and is involved in the first cell and EMS divisions (Gurling et al., 2014; Liro & Rose, 2016; Tsou et al., 2002). Based on the homology of the DEP domain and its predicted GAP domain, the mammalian homolog of TOE-2 is DEPDC7.

Non-muscle myosin is a central component of the actomyosin network and is involved in a wide variety of processes. The non-muscle myosin NMY-2 plays a key role in establishing the polarity of the first cell division and of the NSM, Q.a and Q.p neuroblast divisions (Guo & Kemphues, 1996; Ou et al., 2010; Wei et al., 2020). An interesting complication in generating a unifying model for NMY-2's role in DCSA is that in these divisions, it localizes to different parts of the progenitor cell relative to the cell's polarity. In the Q.a division, NMY-2 localizes to the anterior side, which will become the smaller daughter cell fated to die (Ou et al., 2010). This is similar to its pattern in Drosophila neuroblasts (Tsankova et al., 2017). In the NSM neuroblast, however, NMY-2 localizes to the side that will become the larger surviving NSM daughter cell. This is similar to the *C. elegans* first cell division where NMY-2 initially localizes to the side that will produce the larger AB blast cell (Pacquelet, 2017). However, in Q.p, NMY-2 does not appear to be asymmetric (Ou et al., 2010). Despite the differences in NMY-2 asymmetry, PIG-1 regulates DCSA in all of these *C. elegans* divisions, and has been shown to regulate NMY-2 localization in the NSM and first cell divisions (Chien et al., 2013; Pacquelet et al., 2015; Wei et al., 2020). Considering that in most of these divisions NMY-2 has been shown to play a role in furrow positioning independent of spindle positioning, the fact that the localization of NMY-2's is different in these asymmetric divisions is puzzling.

We used endogenously tagged reporters of NMY-2, TOE-2, and PIG-1 to determine their subcellular localization during the Q.a and Q.p cell divisions in order to better characterize their function. We found that all were asymmetric at the cortex in both the Q.a and Q.p divisions, with TOE-2 and NMY-2 being biased towards the side of the progenitor that will produce the apoptotic daughter, while PIG-1 was biased towards the other side. We used temperature-sensitive *nmy-2* mutants to determine the role of *nmy-2* in these divisions and found that these alleles had only mild effects on the DCSA of the Q.p division and none on the Q.a division. When combined with mutations in *toe-2* or *pig-1,* the *nmy-2* alleles did not significantly alter the Q.a or Q.p DCSA defects of the *toe-2* or *pig-1* mutants but did alter the fate of their daughters. These findings suggest that NMY-2 plays a DCSA-independent role in specifying the fate of the Q.a and Q.p daughter cells.

2.3 Materials and Methods

2.3.1 Strains and Genetics

General handling and culture of nematodes were performed as previously described (Brenner, 1974). N2 Bristol was the wild-type strain, and experiments were performed at 20°C unless otherwise noted.

The following mutations, integrated arrays and endogenously tagged genes were used:

LG I. *nmy-2(ne1490ts, ne3409ts)* (Liu et al., 2010), *nmy-2(cp13)* (*nmy-2::gfp+*LoxP) (Dickinson et al., 2013)

LG II. *toe-2(gm408ok2807)* (Gurling et al., 2014), toe-2(syb1240) (mNeonGreen::*toe-2*) (this study)

LG III. *rdvIs1 [egl-17p::mCherry:his-24 + egl-17p::myristolated mCherry + pRF4]* (Ou et al., 2010)*, casIs165[egl-17p::myr-mCherry; egl-17p::mCherry-TEV-S]* (Zhu et al., 2014).

LG IV. *pig-1(gm280, gm301, gm344)* (Cordes et al., 2006), *pig-1(syb2355)* (*pig-1::mNeonGreen*) (this study)

LGX. *gmIs81 [mec-4p::mCherry, flp-12p::EBFP2, gcy-32p::gfp, egl-17p::gfp]* (Gurling et al., 2014)

2.3.2 Cell Count Protocol

Worms with the *gmIs81* integrated array were grown on Nematode Growth Media (NGM) seeded with OP50 at 15^{o}C until the plates were populated with gravid adult hermaphrodites. Embryos were then collected after incubating the adults in .75 mL of a solution containing 500mM NaOH and 15% bleach until the adults were mostly dissolved, centrifuged to pellet the embryos which were then washed three times in 1.5mL of M9, and then plated on standard NGM plates seeded with OP50 and then transferred to 25^{O}C. After 2-3 days, adult and fourth larval stage (L4) worms were transferred to 3-5 ul of 20mM Sodium Azide in M9 buffer on a 2% agarose pad. Hermaphrodites were scored for the number of observed Q lineage descendants. The number of observed PQR, SDQL and PVM neurons were scored in hermaphrodites with their left side up. The number of observed SDQR and AVM neurons were scored in hermaphrodites with their right side up. The numbers of all five cells were scored in hermaphrodites lying on their dorsal or ventral sides.

2.3.3 Cell Count Analysis

The frequency of extra or missing cells was calculated for each cell type by dividing the number of sides with an extra or missing cell by the number of sides scored. AQRs were excluded from the final analysis as they were difficult to distinguish from other neurons in the head that express GFP in *gmIs81* animals.

The analysis of Q lineage division defects was predicated on the principle that certain cell-fate changes produce unique patterns that cannot be produced by a Q.aa or Q.pp cell that is normally fated to die surviving and adopting the fate of its sister cell or niece. For instance, occasionally Q.p will adopt the fate of Q.a leading to a missing A/PQR and extra SDQL/R or A/PVM cells. Another possibility is a progenitor may fail to divide, leading to the loss of its descendants. To eliminate lineages with these types of defects, each pattern of potential cell counts was analyzed to determine whether the production of extra neurons could result solely from a failure in apoptosis and transformation into its sister cell or niece. Only those lineages were counted in the filtered Q.a and Q.p results. The criteria for excluding a pattern were if a cell was missing or if there were three or more of any cell type. These patterns were arranged into defect categories corresponding with which division had failed. In the final analysis, we used two defect categories, QL.a and QL.p, with the patterns and categories described in Table 2.1. The frequency of each category was determined by the sum of worms exhibiting that category of defect divided by the number of worms scored for that lineage. Specifically, the frequency of QL.p defects was calculated as (# QL.p defective)/(# QL.p defective + # QL.p

normal), while the frequency of QL.a defects was calculated as (# QL.a defective)/(# QL.a defective+ # QL.a normal).

2.3.4 Imaging

Worms with the *gmIs81* integrated array were grown on NGM seeded with OP50 at 15^{o}C until the plates had a large number of embryos and larvae. The plates were then put at 25^{o}C for 4 hours. Worms were then washed off the plates with M9 and transferred to microcentrifuge tubes. They were then spun in a tabletop centrifuge for less than 6 seconds to pellet the larger, adult worms. The supernatant was then transferred using a glass pipette to a fresh microcentrifuge tube. This was then spun for 30 seconds and the supernatant was removed until only ~100µL remained. 2 µL of 1M Sodium azide was added, and the tube was briefly vortexed and spun for 30 seconds. All but ~10 µL of supernatant was removed, and, using a glass pipette, the pellet and remaining M9 + sodium azide were transferred to a 2% agarose slide. To determine the sizes of the daughter cells and the number of Q-derived neurons, the worms were imaged using an Axio Observer Z1 microscope.

For time-lapse imaging, worms were prepared as previously described (Gurling et al., 2014). Time-lapse images of Q neuroblast divisions were captured with seven plane Z-stacks (Z-step: 0.5 µm) in 30-second intervals on a spinning-disk (CSU-X1; Yokogawa) confocal microscope. Images were captured using an EM CCD camera (Evolve; Photometrics) and SlideBook software (Intelligent Imaging Innovations).

2.3.5 Image Analysis

Image analysis was performed using the FIJI package for ImageJ (Schindelin et al., 2012). To measure DCSA, the outlines of recently divided Q.p or Q.a daughters were traced using the lasso select tool in ImageJ, and the area was measured for each cell to determine the ratio. To measure the localization of the endogenously tagged reporters, we identified time points for metaphase, anaphase, telophase and cytokinesis in the time-lapse images and created sum Z-projections of the slices containing the clearest cross-section of the dividing cell. We then performed line scans around the cortex, using the segmented line and plot profile tools in FIJI, measuring the intensity of the endogenously tagged protein in the 488 nm channel and myristoylated mCherry in the 561 nm channel across 3 pixels every 0.167 microns. A line was drawn through either the metaphase plate or cleavage furrow and measurements started at a point where that line intersected the membrane and followed the entire cell cortex as marked by the myristoylated mCherry. The other point intersecting the line of the metaphase plate or cleavage furrow was then marked as were the anterior and posterior sides of the furrow. We also established the background levels of fluorescence by measuring the average intensity in each channel of a section of the body cavity that expressed neither reporter.

2.3.6 Line-scan Modelling

To model the line-scan data, each point was normalized and paired with information about the relevant variables. First, the background intensity for each channel was subtracted from the intensity values. To normalize protein to membrane levels we divided the intensity at 488 nm by the intensity at 561 nm for each point, which we refer to as the Normalized Intensity Ratio.

To compare cells of different sizes, we determined the Normalized Distance by dividing the distance from the start of the measurement by the total distance measured. We also determined the normalized distance between each point and the nearest metaphase plate or cleavage furrow point. Each point was then paired with its Normalized Intensity Ratio, the cell type, the phase of the division, and whether it was anterior or posterior to the division plane.

The line-scan information was used to construct Generalized Mixed Linear Models (GLMMs) using the MCMCglmm package in R (Hadfield, 2010). We used the Normalized Intensity Ratio as the dependent variable, the specific measurement as a random variable, and the Cell Type, the Phase, Anterior vs Posterior, and the distance from the furrow as fixed variables. We also added the interaction terms of Phase::Anterior vs Posterior and Phase::Furrow Distance to account for changes in their effects in different phases. The resulting models allowed us to estimate the effect size of each variable.

In order to determine whether there was a significant difference between the Anterior and Posterior effects during each phase, we used the emmeans R package to calculate the estimated marginal means for the Phase and Anterior vs Posterior interaction term (Lenth, 2019). Using the emmeans pairs function to perform pairwise comparisons between the different estimated effect sizes, we found the difference between the estimated effect sizes for each pair of interaction pairs of Phase and Posterior vs Anterior. The estimated difference between the Anterior and Posterior in each phase is then used to calculate a z-ratio and Tukey adjusted p value. The sign of the estimated difference indicates the direction, with positive values indicating Posterior and negative values indicating Anterior. Plots were made using the gather_emmeans_draws function in the tidybayes R package to generate draws from the marginal posterior distributions of the models and the ggplot2 R package to generate the plots from those draws (Wickham, 2010, 2014).

2.3.7 RNA interference (RNAi)

For *nmy-2* RNAi experiments, the *nmy-2* RNAi bacteria from the Ahringer Library (Kamath & Ahringer, 2003), or L4440 control were grown overnight in LB with 50 µg/ml carbenicillin. 20uL of O/N culture was spread on NGM plates with 50 µg/ml carbenicillin and 1 mM IPTG and allowed to grow at 25^{O}C for 48hrs. Embryos were collected by bleaching and plated on RNAi or L4440 control plates and cell counts were performed as described above.

2.4 Results

2.4.1 NMY-2, TOE-2, and PIG-1 are asymmetrically distributed during the divisions of Q.a and Q.p neuroblasts

The *C. elegans* Q lineage has been a model for studying of asymmetric cell division. The left and right Q cells each undergo a series of divisions along the anterior-posterior axis (A-P) to generate three neurons and two cells fated to die (Sulston & Horvitz, 1977). The Q daughters, Q.a and Q.p, each divide to generate daughter cells that are asymmetric in size and fate (Fig 2.1). Q.a divides to generate a smaller anterior daughter cell that dies and a larger posterior daughter that survives and differentiates into an A/PQR oxygen-sensing neuron. Q.p divides

with the opposite polarity to generate a larger anterior daughter that survives and divides to generate the A/PVM mechanosensory neuron and the SDQR/L interneuron. Because the right and left Q and their descendants migrate in opposite directions, the neurons on the right side (AQR, AVM and SDQR) are in positions anterior to those on the left side (PQR, PVM and SDQL).

The non-muscle myosin NMY-2, the AMPK-family kinase PIG-1, and the DEPDC7 homolog TOE-2 all regulate the asymmetry of the Q.a and Q.p divisions (Cordes et al., 2006; Gurling et al., 2014; Ou et al., 2010). To better understand the roles of these molecules in asymmetric cell division, we took time-lapse images of the Q.a and Q.p divisions in strains containing endogenously tagged NMY-2::GFP, PIG-1::mNeonGreen, or mNeonGreen::TOE-2 (Fig 2.2). We then measured the intensity of the GFP or mNeonGreen at the cortex and normalized it to an mCherry cortical marker. Taking the average normalized intensity of the posterior and anterior sides of the cells, we observed a slight asymmetry of NMY-2::GFP (Fig 2.2A) and mNeonGreen::TOE-2 (Fig 2.2B) towards the side of Q.a or Q.p that will produce the daughter cell fated to die, and strong asymmetry of PIG-1::mNeonGreen towards the side that will produce the daughter cell that survives (Fig 2.2C).

Because both NMY-2 and TOE-2 localize to the cleavage furrow during anaphase and telophase, the ratio of the average intensity of the posterior and anterior could be misleading as identical levels of the protein flanking the furrow combined with the size asymmetry of the daughter cells would result in the smaller side having a higher average intensity. To mitigate this problem, we performed line scans around the cortex and annotated each measured point on the line scan with the intensity normalized by taking the ratio of the intensity of the GFP signal and the intensity of the mCherry cortical marker, the distance from the division plane normalized to the circumference of the cell, the phase of the division, and the positions anterior or posterior to the division plane.

We used this information to construct two GLMMs for each reporter, one for Q.a and one for Q.p, with the normalized intensity ratio as the dependent variable and the other information as fixed variables. We also included interaction terms between the phase and anterior or posterior as well as phase and furrow distance. Interaction terms account for the difference in the effect of one variable based on the value of another variable. In this model, the distribution of the protein with respect to both the A-P bias and proximity to the furrow can vary in different phases. The resulting models allowed us to estimate the effect size of each variable, and, most importantly, the interaction terms allowed us to compare the levels of the reporter at the anterior and posterior within each phase after accounting for the other variables. The resulting models' estimates and parameters can be found in Table S2.1.

Using our model, we found that there was significantly more NMY-2::GFP at the anterior of Q.a during metaphase, anaphase, and telophase. During cytokinesis, NMY-2 was not asymmetric and localized to the cleavage furrow (Fig 2.3A). Our Q.p model had more NMY-2 at the anterior of Q.p at metaphase but no asymmetry during anaphase and telophase. NMY-2 localized asymmetrically to the posterior of Q.p during cytokinesis (Fig 2.3A).

Our model for the distribution of mNeonGreen::TOE-2 was similar to that of NMY-2::GFP: it had a greater anterior distribution throughout the Q.a division though, unlike NMY-2::GFP, mNeonGreen::TOE-2 remained asymmetric during cytokinesis (Fig 2.3B). During the Q.p division, TOE-2 moved steadily toward the posterior as the division progressed (Fig 2.3B). We also found that mNeonGreen::TOE-2 and NMY-2::GFP colocalized in the germline (Fig S2.1). NMY-2 localizes to the lateral membranes that separate at germline nuclei and accumulates at the ring channels that form the pores that connect the germ cells to a central canal, the rachis (Coffman et al., 2016). mNeonGreen::TOE-2 localized to the junction between the germline progenitors Z1 and Z2 and continued to localize to the apical surface of the germline cells through all stages of development (Fig S2.2).

The distribution of TOE-2 reported here differed from previous descriptions of GFP-tagged transgenes. A GFP-tagged *toe-2* cDNA expressed from an *egl-17* promoter accumulated in the nuclei of interphase cells, but we detected no nuclear TOE-2 with the endogenously tagged gene. This is similar to the nuclear localization of the GFP-tagged Arf GEF GRP-1; the endogenous GRP-1 was not detectible with anti-GRP-1 antibodies (Teuliere et al., 2014). The nuclear localization of excess TOE-2 and GRP-1 might ensure that the proteins do not accumulate at the cortex in the interphase cells where they might have deleterious effects.

Our models showed that PIG-1::mNeonGreen was much more asymmetric than either NMY-2::GFP or mNeonGreen::TOE-2, localizing to the posterior of Q.a and the anterior of Q.p during mitosis. For both Q.a and Q.p, the PIG-1::mNeonGreen asymmetry increased as the cells progressed through mitosis (Fig 2.3C).

2.4.2 Temperature-Sensitive *nmy-2* mutants reveal a role in Q lineage ACD

Although the asymmetry of NMY-2 in Q.a has been documented (Ou et al., 2010), we were surprised to find that its distribution was also asymmetric in Q.p during metaphase and cytokinesis. To determine whether NMY-2 also functioned in the Q.p division, we asked whether the two temperature-sensitive *nmy-2* mutants, *nmy-2(ne1490ts)* and *nmy-2(ne3409ts),* had altered Q.a and Q.p DCSA when shifted to 25^{o}C four hours before imaging. We detected a significant decrease in Q.p DCSA in both *nmy-2(ne3409ts)* ($P<0.01$) and *nmy-2(ne1490ts)* mutants ($P<0.05$) compared to the control. Neither had a significant effect on Q.a DCSA. (Fig 2.4C, D).

We also assessed the fates of the QL cell descendants in the mutants by counting the number of PQR, SDQL, and PVM neurons in adult hermaphrodites that had been shifted to 25^{o}C during embryonic development. To determine the number of these cells, we used the *gmIs81* reporter, which labels each cell type with a different fluorescent marker (Gurling et al., 2014). We did not count QR descendants because we could not reliably distinguish AQRs from other neurons expressing GFP in the head. The two *nmy-2* mutants had a low frequency of extra and missing QL descendants (Fig 2.4C). The wild-type control had no extra or missing cells (N=133).

Some of these phenotypes are difficult to interpret and may result from a failure of progenitor cells to divide or cell-fate transformations earlier in the lineage. For example, worms that lack Q.p descendants but have two or more Q.a descendants potentially represent Q.p to Q.a

transformations. Because of these complications, we filtered the cell counts to remove all instances with either a missing cell or three or more of a given cell type. These filtered cell counts were then grouped based on whether they had QL.a or QL.p defects (Table 2.1). Both *nmy-2(ts)* alleles had increased frequencies of QL.a and QL.p defects compared to wild-type (Fig 2.4D). There was not a significant difference between the frequency of QL.a or QL.p defects between *nmy-2(ne1490ts)* and *nmy-2(ne3409ts)* raised at the nonpermissive temperature (Fig 2.4C,D).

2.4.3 Temperature-sensitive *nmy-2* alleles alter *toe-2* mutant Q lineage cell-fate defects but not Q.a or Q.p DCSA

The similar distributions of NMY-2 and TOE-2 during the Q.a and Q.p divisions suggest that they may function together to regulate DCSA. We constructed double mutants with the presumptive null *toe-2(gm408ok2807)* allele and each temperature-sensitive *nmy-2* allele to determine if the two genes function together or in parallel. Consistent with the two genes acting together, there were no significant DCSA differences between the *toe-2* single mutant and either *toe-2; nmy-2(ts)* double mutant (Fig 2.5 A,B). Because the *nmy-2* mutants do not alter Q.a DCSA, the lack of a *toe-2* enhancement is difficult to interpret, but because the mutants do alter Q.p DCSA, the lack of enhancement suggests that *nmy-2* and *toe-2* function together to regulate the size asymmetry of this division.

Our observations of cell fate in the single and double mutants were more complicated. When compared to *toe-2(gm408ok2807)*, the *nmy-2(ne1490ts); toe-2* strain had a significant ($p<0.001$) increase in the frequency of extra SDQL and PVM neurons and a decrease in the frequency of extra PQR neurons (Fig 2.5C). After filtering, there was a similar decrease in QL.a defects and an increase in QL.p defects in the double mutants (Fig 2.5 D). The *nmy-2(ne3409ts); toe-2* strain had weaker effects: a significant ($P<0.05$) increase in the frequency of extra SDQL cells and a decrease in the frequency of extra PQR cells (Fig 2.5C). However, the *nmy-2(ne3409ts); toe-2* strain was not significantly different from *toe-2(gm408ok2807)* in the frequency of QL.a or QL.p defects after filtering (Fig 2.5 D).

The difference between the results for the temperature-sensitive alleles led us to repeat the experiments with *nmy-2* RNA interference (RNAi) (Supplementary Table 2.1). We observed that *nmy-2* RNAi treatment of *toe-2(gm408ok2807)* resulted in an increase of both the Q.a and Q.p cell-fate defects relative to the *toe-2(gm408ok2807)* RNAi control. This observation is consistent with our Q.p findings for the *toe-2* double mutant with *nmy-2(ne1490ts)* allele. Unlike the suppression of the *toe-2* Q.a defects by *nmy-2(ne1490ts), nmy-2* RNAi enhanced the Q.a defects of *toe-2.*

The lack of a significant enhancement of the *toe-2* mutant by the *nmy-2(ne3409ts)* mutation suggests that this allele is weaker than the *nmy-2(ne1490ts)* allele. To test this hypothesis, we treated the *nmy-2* mutants with *nmy-2 RNAi* and found both *nmy-2(ne1490ts)* and *nmy-2(ne3409ts)* resulted in a significant increase in the frequency of Q.p defects at the nonpermissive temperature, suggesting that both mutations reduce but do not eliminate *nmy-2* function at the nonpermissive temperature (Table S2.2). Because there was no effect on the

toe-2 Q.a defects by the *nmy-2(ne3409ts)* mutation and *nmy-2* RNAi enhanced these defects, the reason for the suppression of these defects by *nmy-2(ne1490ts)* is unclear. The *nmy-2(ne1490ts)* mutation could alter *nmy-2* function in a unique way or the strain could have a second mutation that leads to the suppression.

2.4.4 Temperature-sensitive nmy-2 alleles suppress pig-1(gm301) Q.a cell fate defects while not significantly altering Q.a DCSA

Our finding that PIG-1 and NMY-2 localized to opposite sides of Q.a suggests that these two molecules play different roles in these cells. To determine how *pig-1* and *nmy-2* interact, we constructed *nmy-2; pig-1(gm301)* double mutants and scored the single and double mutants for Q.a and Q.p DCSA defects and the presence or absence of Q-lineage neurons. There were no significant differences in DCSA of either Q.a or Q.p between *pig-1* single and *nmy-2(ts); pig-1* double mutants (Fig 2.6 A, B). Both double mutant strains had a significant decrease in the frequency of extra PQR neurons and QL.a-specific defects when raised at the nonpermissive temperature of 25^{o}C. (Fig 2.6 C, D). The *pig-1* single and the *nmy-2; pig-1* double mutants displayed similar Q.p defects.

The significant increase in SDQLs in the *nmy-2(ne1490ts); pig-1(gm301)* strain compared to the *pig-1(gm301)* strain is potentially due to what is referred to by Mishra et. al (Mishra et al., 2018) as an increase in mitotic potential (Fig 2.6C). Specifically, in instances where QL.pp survives in *pig-1(gm301)*, it divides 46.2% of the time, while in *nmy-2(ne1490); pig-1(gm301)* it divides significantly ($P<0.001$) more frequently, 63.8% of the time (Table S2.3).

2.4.5 Time-lapse imaging of a *pig-1(gm344)* mutant background shows a reversal of NMY-2::GFP asymmetry in Q.a and Q.p

To further examine the potential interaction effects between *nmy-2* and *pig-1*, we constructed a *nmy-2::GFP; pig-1(gm344)* strain. We observed a reversal of the NMY-2::GFP asymmetry, with more posterior NMY-2::GFP in Q.a during metaphase, telophase and cytokinesis (Fig 2.7A,C), and a more anterior NMY-2::GFP in Q.p throughout mitosis (Fig 2.7 B,D). The Q.a reversal differs from a previous report that observed a loss of NMY-2::GFP asymmetry in a *pig-1* mutant (Ou et al., 2010).

2.5 Discussion

2.5.1 NMY-2 is asymmetric in Q.a and Q.p and functions in Q.p DCSA

Our results for NMY-2 are interesting in that they do not align fully with previously reported findings. In particular, the experiments of Ou et al. using a GFP-tagged NMY-2 transgene showed significant asymmetry of the GFP::NMY-2 in Q.a but not Q.p (Ou et al., 2010). The authors also performed Chromophore Assisted Laser Inactivation (CALI) experiments where they inactivated the GFP::NMY-2 transgene at the anterior of Q.a or the posterior of Q.p during late anaphase (Ou et al., 2010). In Q.a, they saw that this perturbation caused an attenuation, loss, or reversal of DCSA and an increased rate of survival and differentiation of Q.aa. However, they observed no change in Q.p DCSA (Ou et al., 2010). This led them to conclude that *nmy-2* primarily regulates Q.a DCSA.

By contrast, we observed that endogenously tagged NMY-2::GFP exhibited asymmetry in both divisions, with a bias towards the anterior throughout the Q.a division and an increasing bias towards the posterior after an initial anterior bias in the Q.p division. Our experiments with temperature-sensitive *nmy-2* mutants showed no significant change in Q.a DCSA and a significant reduction in Q.p DCSA. Supporting this observation, we observed a higher frequency of extra Q.p lineage cells compared to Q.a.

What could explain these differences? Excess NMY-2 transgene expression could make it harder to observe the more subtle asymmetry we observed in Q.p imaging of the endogenous *nmy-2* tagged with GFP. The transgene used in the Ou et al. study contains multiple copies of *nmy-2* expressed from a heterologous promoter (Nance et al., 2003). A possible confounding factor in the CALI experiments is the presence of endogenous NMY-2. Whereas the CALI experiments would still produce an imbalance in contractile forces by reducing the levels of NMY-2 in the inactivated region, the expression of untagged NMY-2 makes it likely that NMY-2 activity or the activity of other nearby molecules affected by CALI still persists in the irradiated areas. The lack of a CALI result with irradiation of the posterior of Q.p could reflect less sensitivity to altered levels of NMY-2 than the anterior of Q.a.

Given the asymmetry of NMY-2 in Q.a and the results of CALI experiments reported by Ou et al., we were surprised to find no DCSA phenotype for Q.a in the *nmy-2* mutants. The lack of a Q.a DCSA phenotype could result from residual *nmy-2* function in the mutants: the low level of NMY-2 activity remaining would be sufficient to prevent loss of asymmetry in Q.a.

In Drosophila neuroblasts, as in *C. elegans* Q.a and Q.p, more non-muscle myosin localizes to the side that will produce the smaller cell. In the Drosophila neuroblast, this localization is thought to produce a cortical contraction that prevents membrane extension (Connell et al., 2011). In the *C. elegans* NSM neuroblast and the first cell division, NMY-2 localizes to the opposite side of the dividing cell, the side that will produce the larger daughter cell (Tsankova et al., 2017). In the NSM neuroblast division, the *nmy-2(ne3409ts)* mutation results in a complete loss of DCSA. The authors proposed that NMY-2 creates cortical flows that are required to establish the gradient of cell-fate determinants and increase cortical contractility on

the ventral side, which will produce the larger daughter cell (Wei et al., 2020). This model contrasts with the models of cortical contractility on the side that produces the smaller daughter cell. Further experiments are needed to determine which model would be correct in the context of the Q lineage.

2.5.2 NMY-2 has a role in Q-lineage fate determination that is independent of its role in DCSA

The temperature-sensitive NMY-2 alleles caused defects in cell-fate determination in both Q.a and Q.p despite having no or minimal impact, respectively, on the DCSA of those divisions. These findings suggest that NMY-2 has a DCSA-independent role in cell fate determination in the Q.a and Q.p divisions. The finding that NMY-2 regulates cell fate has also been observed in the NSM neuroblast division. Besides eliminating DCSA, the *nmy-2(ne3409ts)* mutation disrupted the gradient of CES-1, a Snail-like transcription factor and cell-fate determinant (Wei et al., 2020).

We observed that the endogenously tagged mNeonGreen::TOE-2 and NMY-2::GFP reporters exhibited similar localization patterns in the Q.a and Q.p divisions, with both being biased towards the side that will produce the daughter cell fated to die as well as to the cleavage furrow. This localization suggests that they may have related functions. Consistent with this possibility, double mutants of *toe-2* and the temperature-sensitive alleles of *nmy-2* exhibit no increase in DCSA in either the Q.a or Q.p divisions when compared to *toe-2* on its own but did have differences in specifying the fate of their descendants. In particular, both *nmy-2(ts)* mutations increased the frequency of the *toe-2* mutant QL.p defects. The interactions between the *nmy-2* and *toe-2* mutations on the fate of the Q.a descendants were variable and difficult to interpret. The Q.p interaction is consistent with a role for NMY-2 in regulating cell fate independent of its role in DCSA. A DCSA-independent role is further supported by the finding that both *nmy-2(ts)* mutations suppressed the frequency of QL.a defects in *pig-1(gm301)* mutants without significantly altering QL DCSA.

A possible mechanism for NMY-2's function in specifying fate in the Q lineage is to distribute cell fate determinants, as was shown for CES-1 in the NSM neuroblast (Wei et al., 2020). This has also been observed in Drosophila neuroblasts where non-muscle myosin is required for the basal distribution of two cell-fate determinants, Prospero and Numb (Barros et al., 2003). Another possible explanation would be an indirect effect wherein the *nmy-2(ts)* strains may have defects that slow cytokinesis or abscission, potentially resulting in cell fate determinants losing asymmetry due to a persisting connection between the daughter cells. This is supported by the observation of persistent intercellular bridges between the daughter cells of both Q.a and Q.p in strains containing the *nmy-2(ts)* alleles (Fig S2.3) as well as the fact that the original characterization of the *nmy-2(ts)* alleles reported that the cleavage furrow of the first embryonic division would halt or regress when the embryo was shifted to the non-permissive temperature (Liu et al., 2010).

2.5.3 PIG-1 is asymmetric in Q.a and Q.p and regulates NMY-2 localization in those divisions.

Previous studies using a *Ppig-1::pig-1::gfp* transgene showed that PIG-1::GFP localized to the cortex and centrosomes, but did not report any asymmetry in the Q lineage (Chien et al., 2013).

The endogenously tagged PIG-1::mNeonGreen showed cortical localization as well as a clear asymmetry towards the side of the neuroblast that would produce the daughter cells fated to live during both the Q.a and Q.p divisions.

Using double mutant strains of *pig-1* and the temperature-sensitive *nmy-2* alleles, we observed no significant change in surviving QL.pp cells compared to *pig-1* on its own. We observed a shift of lineages that produced an extra SDQL and PVM to those that produced both extra SDQL and PVM and interpret this as an increase in mitotic potential. By contrast, there was a significant decrease in the frequency of surviving QL.aa cells in both *nmy-2(ne1490ts); pig-1* and *nmy-2(ne3409ts); pig-1* when compared to *pig-1* on its own.

We were surprised to observe a reversal of the NMY-2::GFP localization pattern in both Q.a and Q.p in the *pig-1* mutant background: using a transgene that expresses NMY-2::GFP, both Ou et al. and Wei et al. observed a loss of NMY-2 asymmetry in a *pig-1* mutant. It is noteworthy that there was no significant alteration in DCSA in either division for either *nmy-2; pig-1* double mutant strain when compared to the *pig-1* single mutant strain.

In the NSM neuroblast division, *nmy-2* functions downstream of *pig-1* (Wei et al., 2020). The authors showed that NMY-2 lost its cortical asymmetry in the NSM and identified two phosphorylation sites on NMY-2 that were partially dependent on PIG-1 for phosphorylation. They also found that phosphomimetic NMY-2 was able to partially rescue the loss of PIG-1 in the NSM division.

An interesting set of future experiments would be to determine if PIG-1 has the same pattern of cortical asymmetry towards the larger side of other asymmetric divisions throughout *C. elegans* development, as we know from the difference between the localization of NMY-2 in the NSM neuroblast division and the Q lineage divisions that NMY-2's localization pattern is not constant.

2.6 Figures

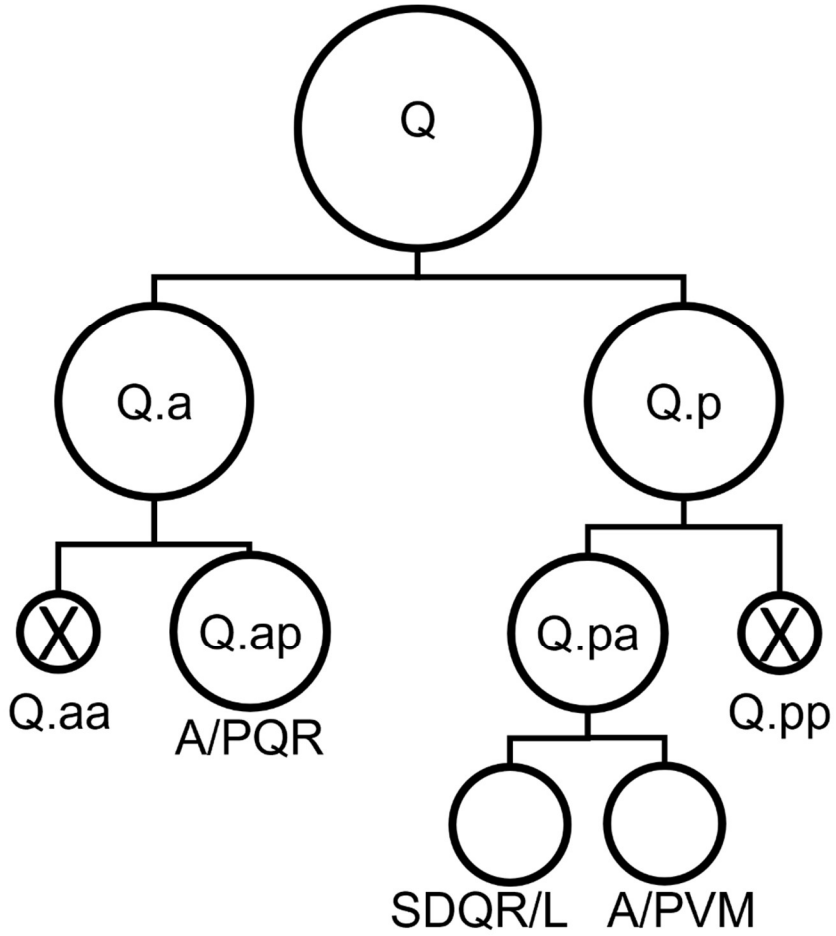

Fig 2.1. The *C. elegans* Q neuroblast divisions.
The Q neuroblast divides to produce Q.a and Q.p, which divide to produce anterior (Q.aa or Q.pa) and posterior (Q.ap or Q.pp) daughter cells. In the Q.a division, the anterior daughter, Q.aa, is smaller and apoptotic. In the Q.p division, the posterior daughter, Q.pp, is smaller and apoptotic.

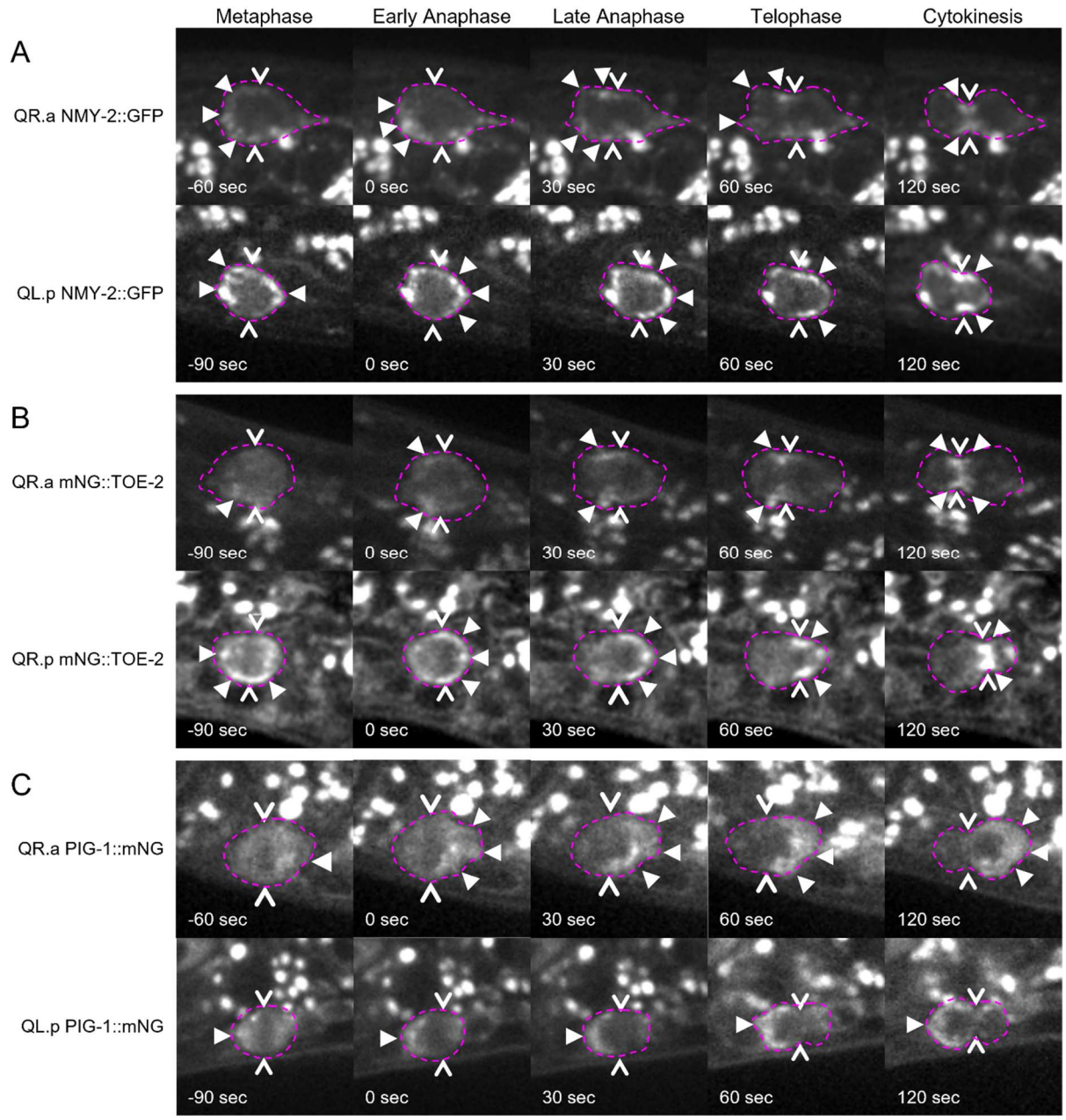

Fig 2.2. Time-lapse images of endogenously tagged DCSA proteins in the Q.a and Q.p divisions.

A-C) Time-lapse imaging of QR.a and QL.p divisions in A) NMY-2::GFP, B) mNeonGreen::TOE-2, and C) PIG-1::mNeonGreen. Dotted lines outline the membrane of the cells. Filled arrowheads indicate areas of higher GFP or mNeonGreen signal, open arrowheads indicate the division plane.

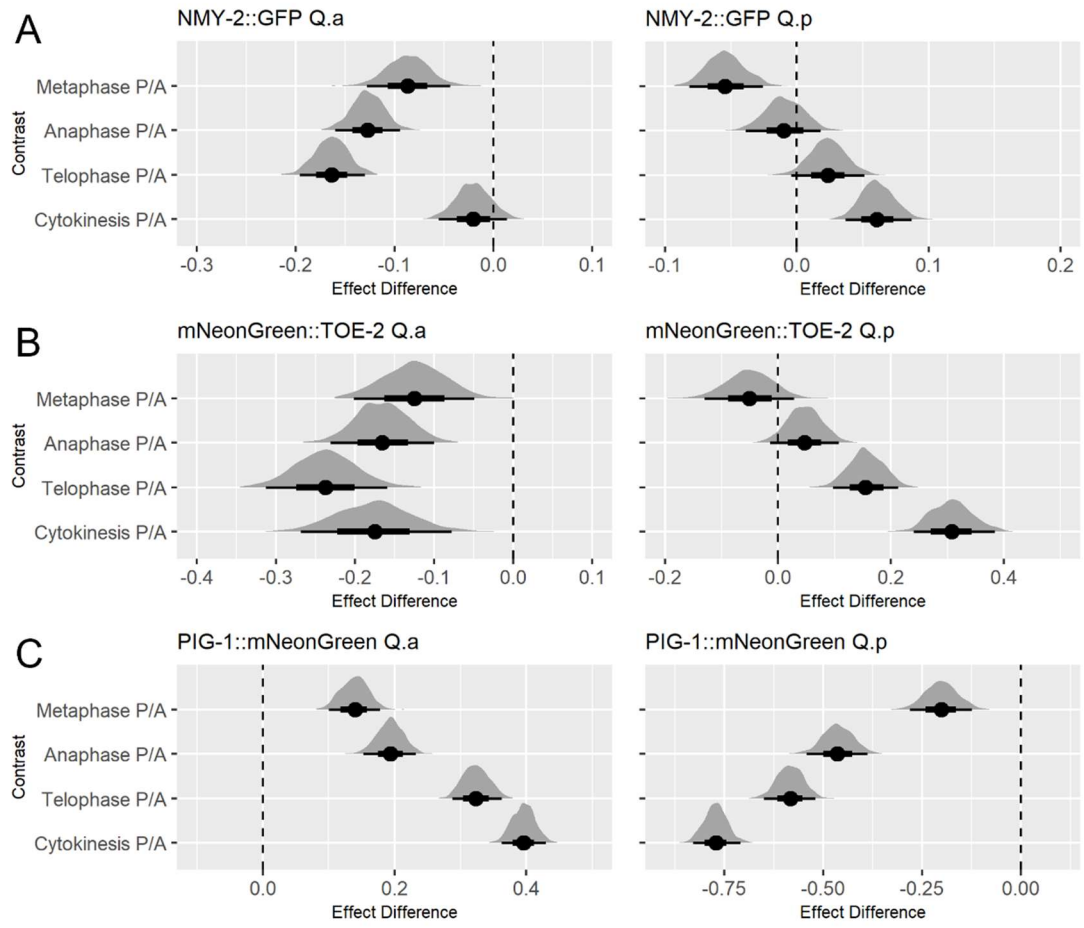

Fig 2.3. Line scan modelling analysis of endogenous reporters shows asymmetry in Q.a and Q.p divisions.

A-C) Modelling analysis comparing anterior and posterior effect in Q.a and Q.p in Metaphase, Anaphase, Telophase and Cytokinesis for A) NMY-2::GFP, B) mNeonGreen::TOE-2, and C) PIG-1::mNeonGreen. The black bars represent the confidence intervals, while the distributions represent the frequency of draws of that value. Larger negative values indicate greater anterior effect, larger positive values indicate greater posterior effect.

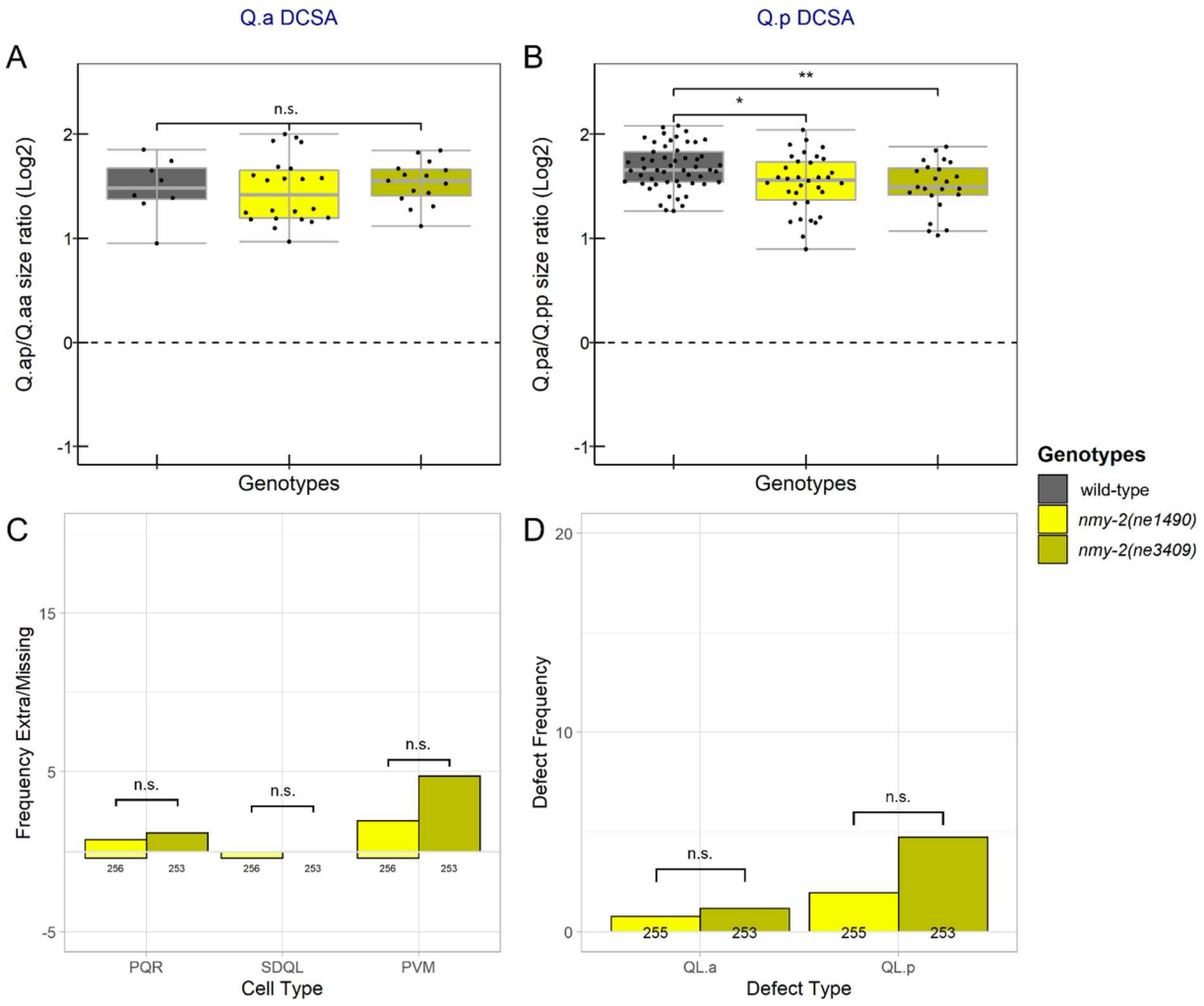

Fig 2.4. DCSA and cell-fate defects in temperature-sensitive *nmy-2* mutants.

A,B) Box plots of the area ratios of A) Q.ap/Q.aa and B) Q.pa/Q.pp divisions in control and *nmy-2*(ts) mutants. C) Frequency of extra (positive y axis) and missing (negative y axis) Q lineage cells. D) Frequency of extra cell defects that could be explained by survival of QL.aa or QL.pp. (C, D) Below each bar are the number of lineages scored. *: P<0.05, **: P<0.01, ***: P<0.001, n.s.: P>0.05.

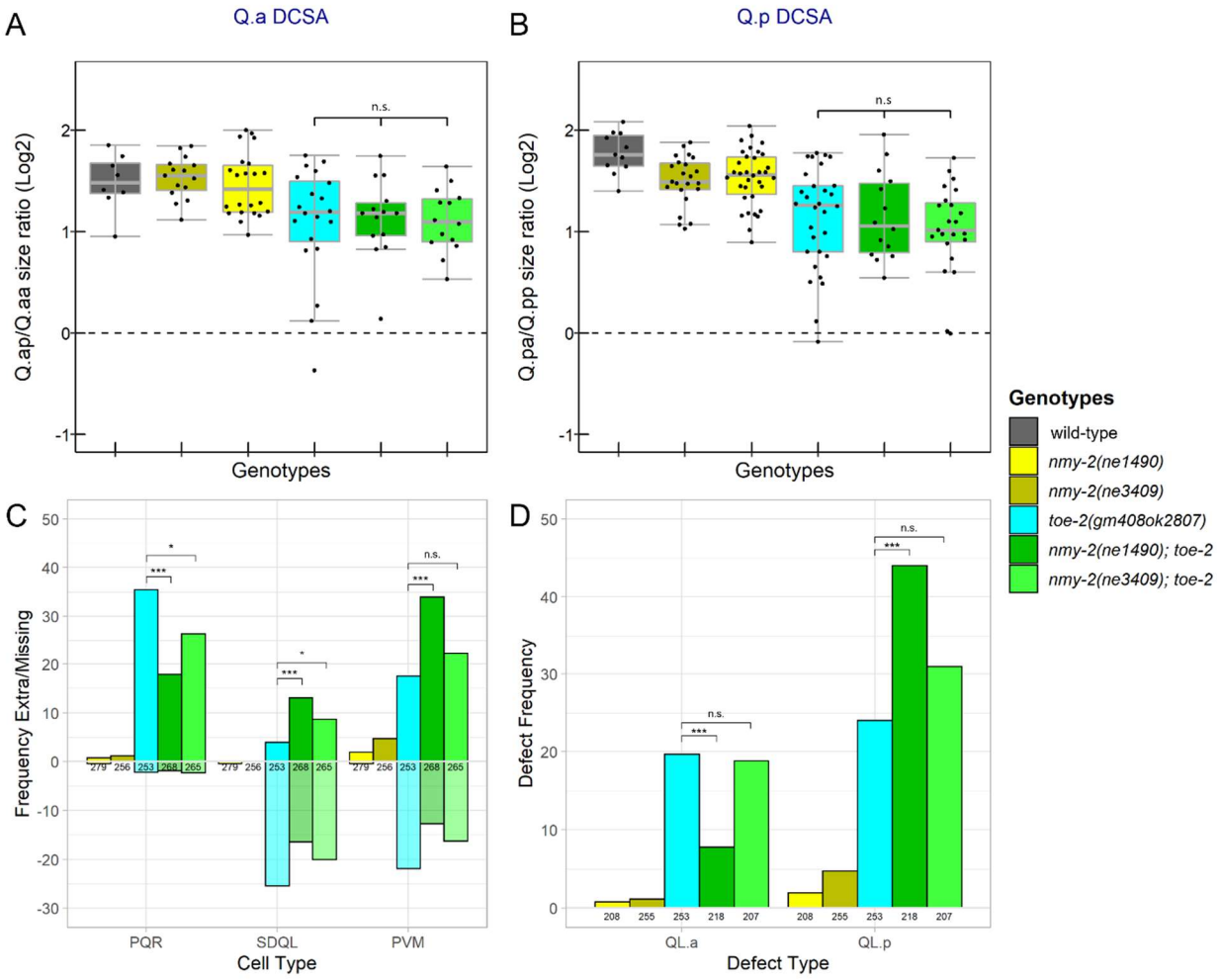

Fig 2.5. Temperature-sensitive *nmy-2* mutants enhance *toe-2* Q lineage cell fate but not DCSA defects.

A, B) Box plots of area rations of A) Q.ap/Q.aa and B) Q.pa/Q.pp divisions. C) Frequency of extra (positive y axis) and missing (negative y axis) QL lineage cells. D) Frequency of extra cell defects that could be explained by survival of QL.aa or QL.pp with no other cell-fate transformations. (C, D) Below each bar are the number of lineages scored. *: P<0.05, **: P<0.01, ***: P<0.001, n.s.: P>0.05.

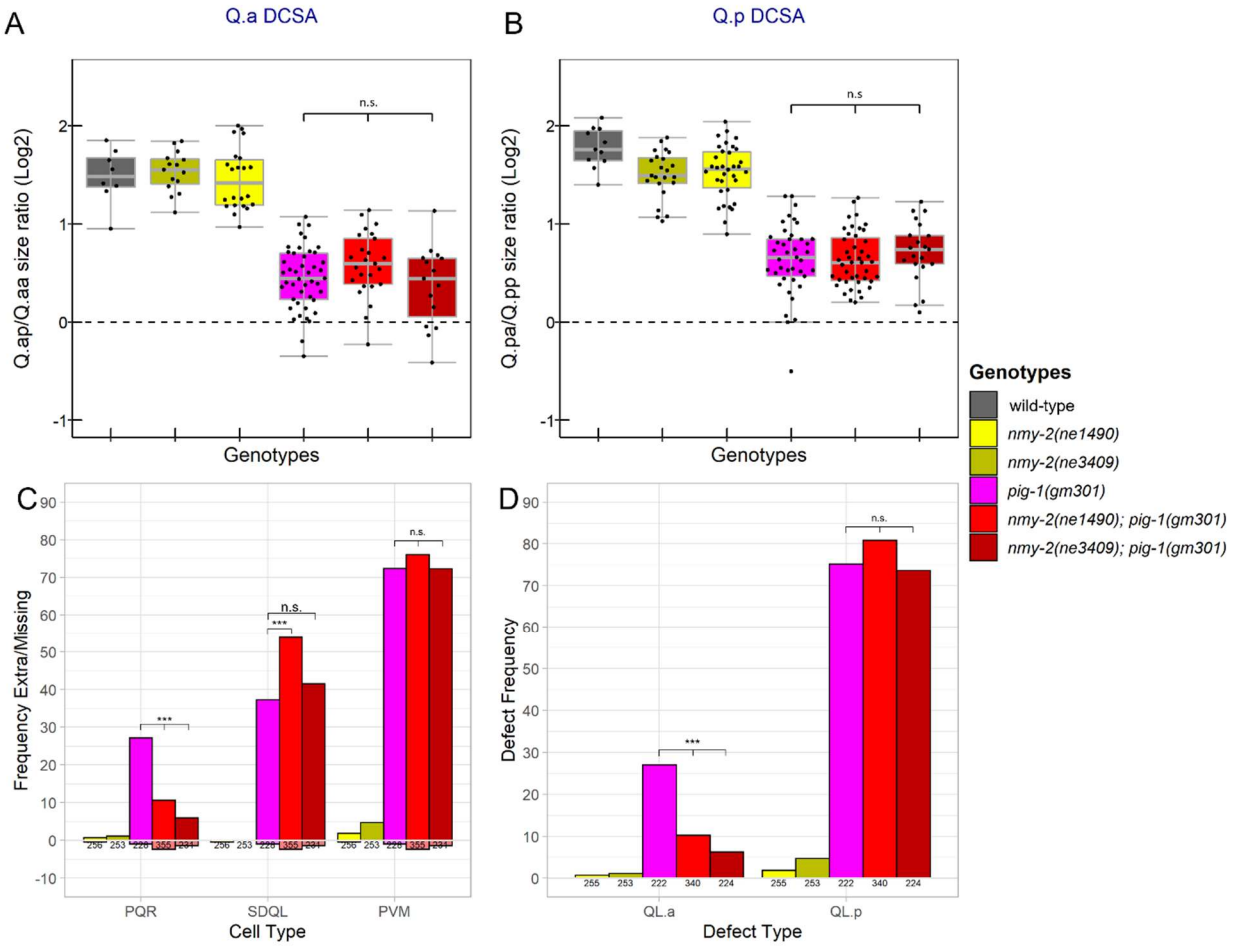

Fig 2.6. Temperature-sensitive *nmy-2* alleles suppress *pig-1(gm301)* Q.a cell fate defects while not significantly altering Q.a DCSA.

A,B) Box plots of the area ratios of A) Q.ap/Q.aa and B) Q.pa/Q.pp divisions. C) Frequency of extra (positive y axis) and missing (negative y axis) QL lineage cells. D) Frequency of extra cell defects that could be explained by survival of QL.aa or QL.pp. (C, D) Below each bar are the number of lineages scored. *: P<0.05, **: P<0.01, ***: P<0.001, n.s.: P>0.05.

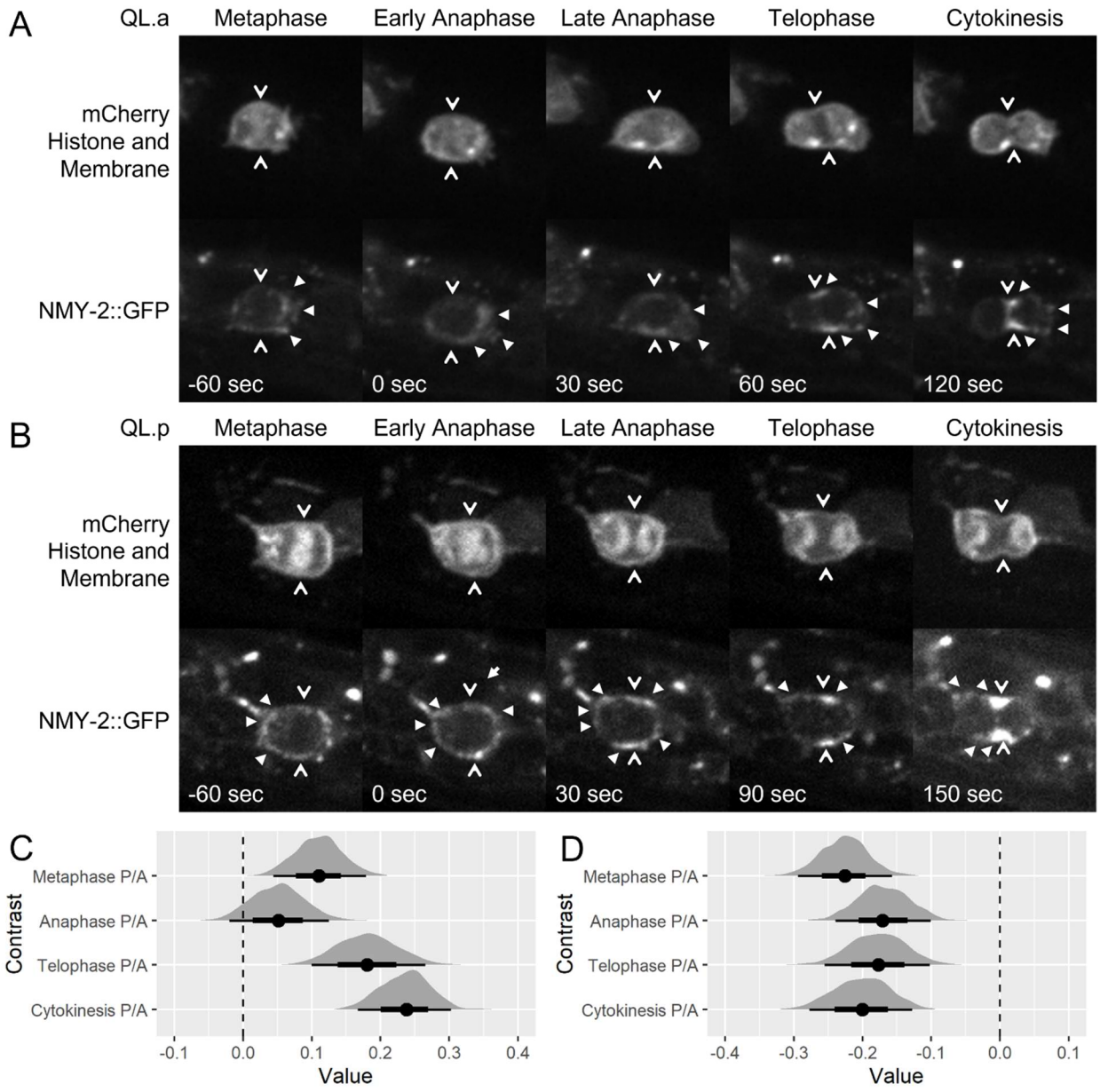

Fig 2.7. Time-lapse images of NMY-2::GFP in *pig-1(gm344)* background shows a reversal of NMY-2::GFP asymmetry in Q.a and Q.p.

A) QR.a and B) QR.p live imaging of NMY-2::GFP in the *pig-1(gm344)* background. Filled arrows indicate areas of higher NMY-2::mNeonGreen signal, open arrows indicate the division plane. C, D) Line scan modelling analysis of C) Q.a and D) Q.p Posterior vs Anterior effect size difference. Negative values indicate a greater posterior effect, positive values indicate a greater anterior effect.

2.7 Supplementary Figures

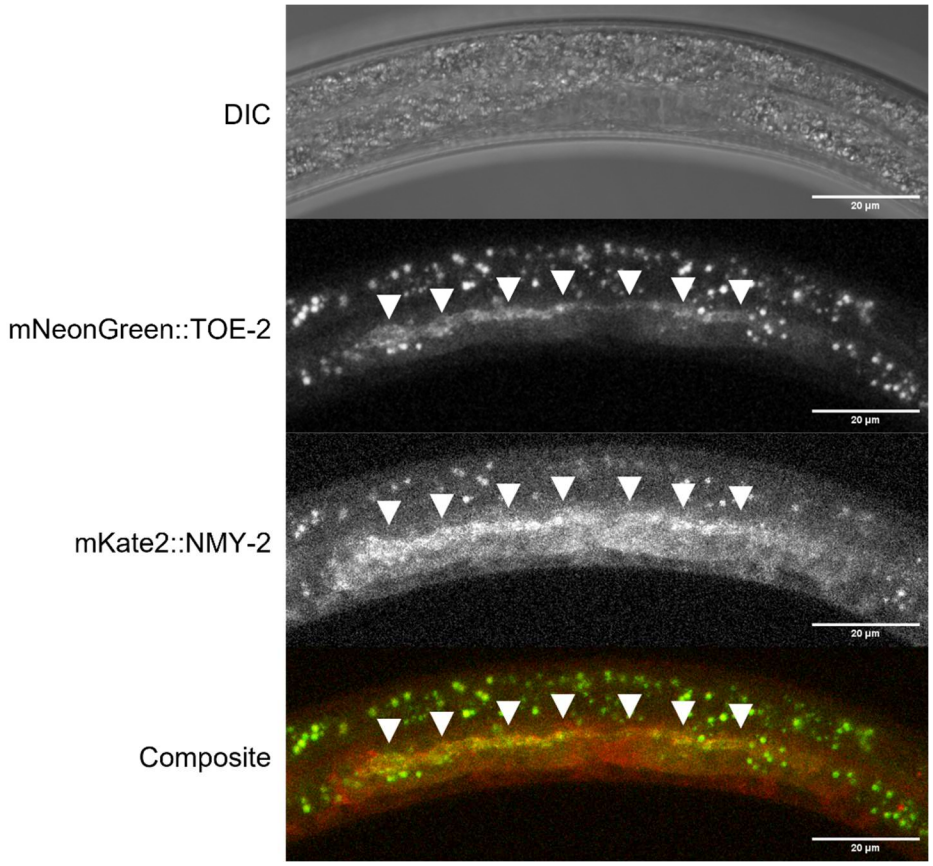

Fig S2.1. TOE-2 and NMY-2 are present at the apical germline.
Confocal images of endogenously tagged TOE-2 and NMY-2 in a third larva stage (L3) hermaphrodite. Both proteins are expressed in the germline and accumulate at the apical surface of the germline cells. Arrowheads indicate the apical germline.

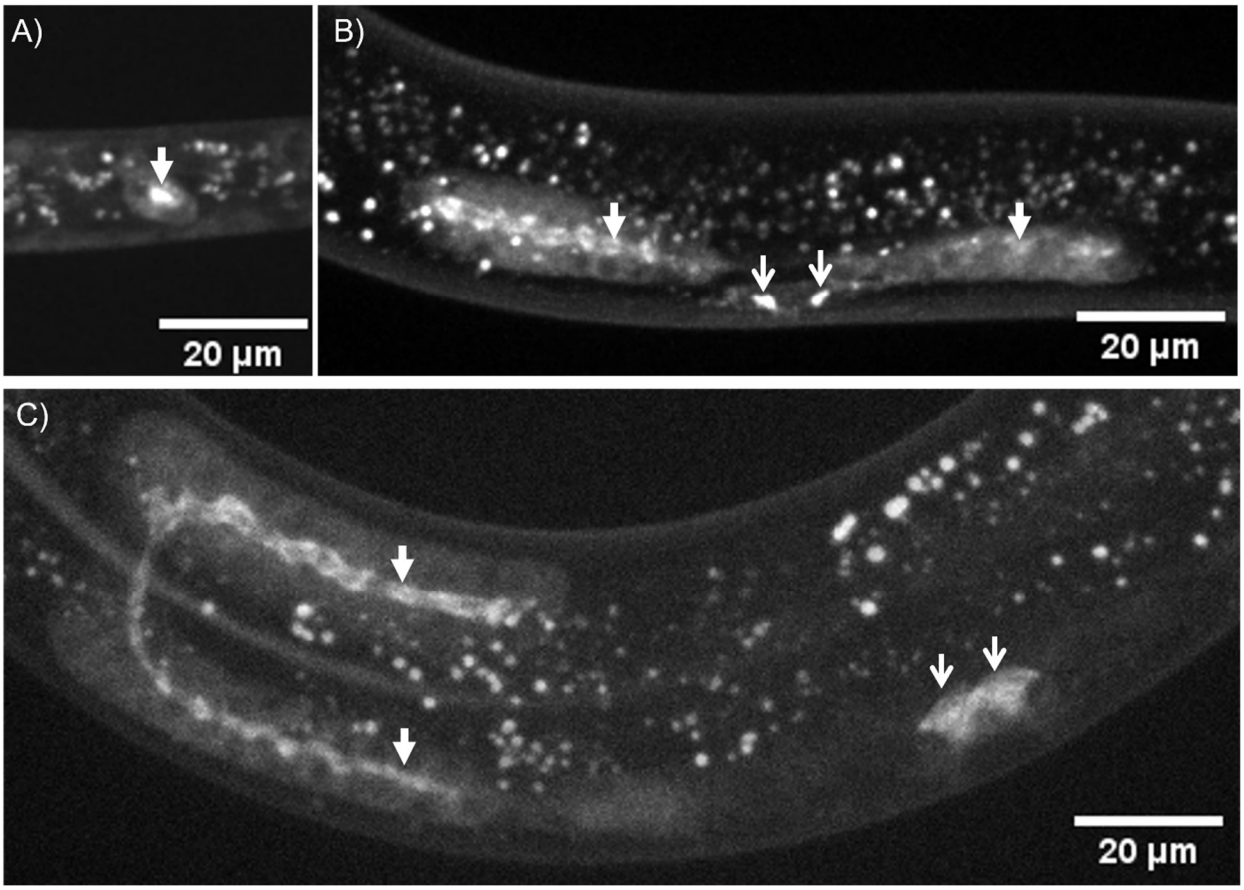

Fig S2.2. Confocal imaging of endogenously tagged TOE-2 localizing to the apical surface of the germ cells.

A) mNeonGreen::TOE-2 in a first larval (L1) stage hermaphrodite. Closed arrowhead indicates mNeonGreen::TOE-2 at the point of contact between Z2 and Z3. B) mNeonGreen::TOE-2 in an L3 stage hermaphrodite. Closed arrowheads indicate localization of mNeonGreen::TOE-2 to the apical surface of the germline cells. Open arrowheads indicate mNeonGreen::TOE-2 localization to unknown cells near the vulva. C) mNeonGreen::TOE-2 in a fourth larval (L4) stage hermaphrodite. Closed arrowheads indicate mNeonGreen::TOE-2 localization to the apical surface of the germline cells. Open arrowheads indicate the positions of unknown cells near the vulva.

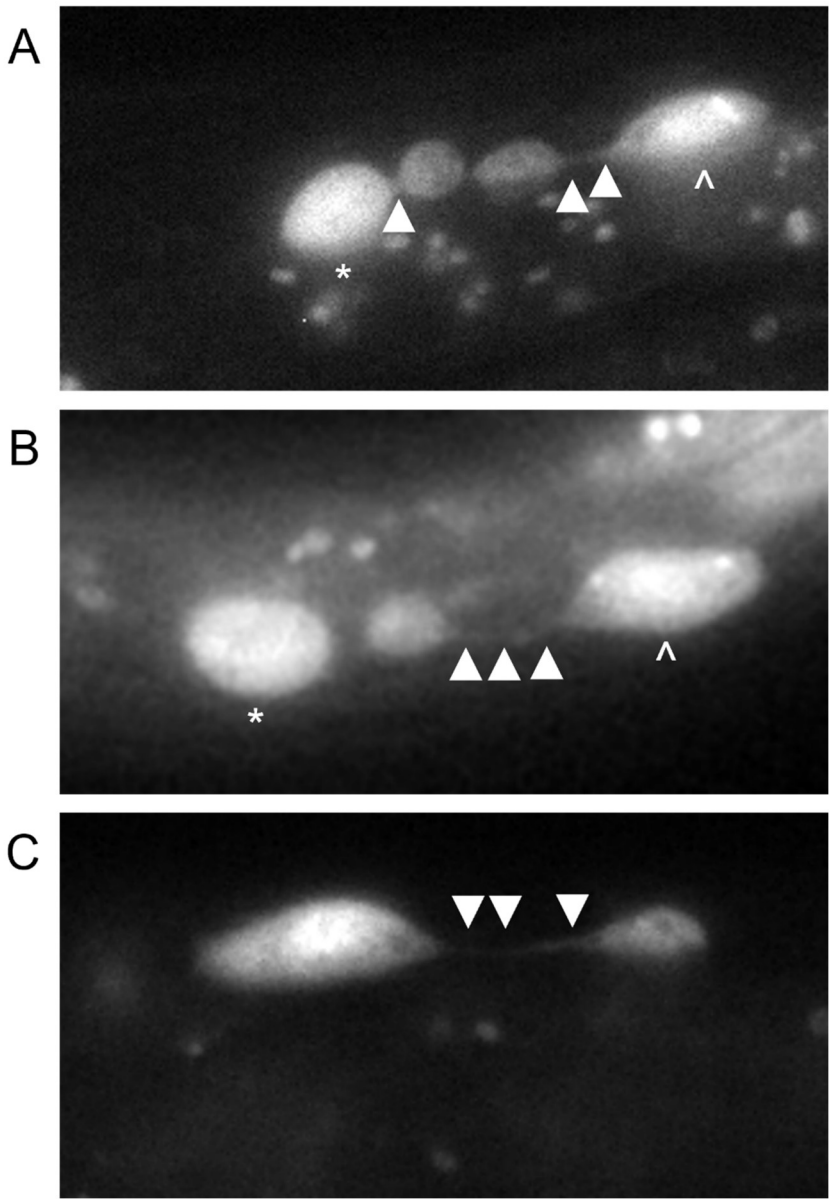

Fig S2.3. Intercellular bridges persist between Q lineage neuroblasts in *nmy-2(ts)* mutants. Anterior is to the left in A-C. A) QL.a and QL.p cells in an nmy-2(ne3409ts) mutant raised at the nonpermissive temperature with persistent intercellular bridges between their daughter cells. The cells on the left are the QL.p daughters. The QL.a daughters are more posterior because QL.a migrated past the Q.p cell before dividing. B) QL.a cell in an nmy-2(ne3409ts) mutant raised at the nonpermissive temperature with a persistent intercellular bridge between its daughter cells. The cell to the left is an undivided QL.p cell. C) QR.p cell in nmy-2(ne1490ts) mutant raised at the nonpermissive temperature with a persistent intercellular bridge between its daughter cells. Arrowheads indicate intercellular bridges, * indicates the QL.p and ^ indicates the QL.a cell.

2.8 Tables:

Table 2.1: QL lineage Cell count defect filtering

# CELLS ON LEFT SIDE			DEFECT PRESENT?	
PQR	**SDQL**	**PVM**	**QL.a**	**QL.p**
1	1	1	No	No
1	1	2	No	Yes
1	2	1	No	Yes
1	2	2	No	Yes
2	1	1	Yes	No
2	1	2	Yes	Yes
2	2	1	Yes	Yes
2	2	2	Yes	Yes

The filtering method used to determine what cell count patterns corresponded to each defect type for the left side Q lineage neurons while excluding all cases requiring a cell fate transformation beyond the survival of the QL.aa or QL.pp cell.

2.9 Supplementary Tables:

Table S2.1. Coefficient Estimates for models of the distribution of NMY-2::GFP, PIG-1::mNeonGreen, and mNeonGreen::TOE-2 during the Q lineage divisions

	Genotype	*nmy-2::GFP*		*pig-1::mNeonGreen*		*mNeonGreen::toe-2*		*nmy-2::GFP; pig-1(gm344)*	
	Cell	Qa		Qa		Qa		Qa	
Variable	Term Type	Estimate [95% CI]	pMCMC	Estimate [95% CI]	pMCMC	Estimate [95% CI]	pMCMC	Estimate [95% CI]	pMCMC
Intercept	fixed	0.582 [0.348, 0.808]	0.001	0.374 [0.127, 0.569]	0.014	0.771 [0.051, 1.474]	0.054	0.494 [0.022, 0.924]	0.038
Posterior	fixed	-0.086 [-0.13, -0.047]	0.001	0.139 [0.102, 0.179]	0.001	-0.125 [-0.203, -0.052]	0.002	0.11 [0.04, 0.172]	0.002
Furrow Distance	fixed	0.351 [0.078, 0.641]	0.022	1.266 [1.006, 1.535]	0.001	-0.868 [-1.326, -0.357]	0.001	1.253 [0.85, 1.644]	0.001
Anaphase	fixed	0.097 [0.039, 0.154]	0.001	0.039 [-0.027, 0.096]	0.228	0.293 [0.186, 0.399]	0.001	0.069 [-0.028, 0.183]	0.19
Telophase	fixed	0.193 [0.136, 0.253]	0.001	0.004 [-0.049, 0.066]	0.862	0.606 [0.494, 0.741]	0.001	0.386 [0.278, 0.503]	0.001
Cytokinesis	fixed	0.251 [0.194, 0.308]	0.001	0.018 [-0.039, 0.08]	0.544	0.8 [0.665, 0.925]	0.001	0.818 [0.707, 0.92]	0.001
Posterior: Anaphase	fixed	-0.041 [-0.094, 0.009]	0.138	0.054 [-0.006, 0.11]	0.066	-0.041 [-0.153, 0.048]	0.412	-0.059 [-0.147, 0.042]	0.242
Posterior: Telophase	fixed	-0.077 [-0.131, -0.023]	0.004	0.185 [0.13, 0.236]	0.001	-0.112 [-0.208, 0.007]	0.05	0.071 [-0.034, 0.177]	0.174
Posterior: Cytokinesis	fixed	0.066 [0.018, 0.12]	0.02	0.257 [0.206, 0.311]	0.001	-0.051 [-0.178, 0.062]	0.386	0.126 [0.034, 0.229]	0.01
Furrow Distance: Anaphase	fixed	-0.582 [-0.914, -0.229]	0.001	-0.394 [-0.801, -0.049]	0.036	-1.685 [-2.403, -1.109]	0.001	-0.452 [-1.031, 0.182]	0.162
Furrow Distance: Telophase	fixed	-1.216 [-1.556, -0.861]	0.001	-1.113 [-1.449, -0.726]	0.001	-2.801 [-3.506, -2.149]	0.001	-3.038 [-3.666, -2.398]	0.001
Furrow Distance: Cytokinesis	fixed	-2.092 [-2.472, -1.774]	0.001	-1.366 [-1.725, -1.04]	0.001	-3.669 [-4.412, -2.961]	0.001	-6.424 [-7.019, -5.756]	0.001
Cell	random	0.133 [0.04, 0.289]	NA	0.066 [0.003, 0.234]	NA	0.617 [0.016, 1.893]	NA	0.343 [0.058, 0.873]	NA
units	residual	0.068 [0.065, 0.071]	NA	0.041 [0.039, 0.044]	NA	0.119 [0.11, 0.128]	NA	0.174 [0.164, 0.186]	NA

	Cell	Qp		Qp		Qp		Qp	
Variable	Term Type	Estimate [95% CI]	pMCMC	Estimate [95% CI]	pMCMC	Estimate [95% CI]	pMCMC	Estimate [95% CI]	pMCMC
Intercept	fixed	0.402 [0.261, 0.54]	0.001	1.072 [0.442, 1.608]	0.001	0.797 [0.396, 1.18]	0.002	0.809 [0.226, 1.496]	0.024
Posterior	fixed	-0.054 [-0.082, -0.026]	0.001	-0.201 [-0.277, -0.121]	0.001	-0.05 [-0.132, 0.027]	0.214	-0.226 [-0.296, -0.162]	0.001
Furrow Distance	fixed	0.571 [0.388, 0.757]	0.001	0.13 [-0.208, 0.469]	0.416	-0.258 [-0.744, 0.22]	0.288	1.455 [1.082, 1.873]	0.001
Anaphase	fixed	0.034 [-0.007, 0.079]	0.132	0.244 [0.154, 0.344]	0.001	0.257 [0.151, 0.381]	0.001	0.226 [0.116, 0.323]	0.001
Telophase	fixed	0.144 [0.103, 0.186]	0.001	0.277 [0.171, 0.364]	0.001	0.405 [0.292, 0.506]	0.001	0.591 [0.471, 0.692]	0.001
Cytokinesis	fixed	0.307 [0.268, 0.349]	0.001	0.256 [0.169, 0.341]	0.001	0.53 [0.423, 0.65]	0.001	0.844 [0.733, 0.958]	0.001
Posterior: Anaphase	fixed	0.045 [0, 0.081]	0.036	-0.262 [-0.369, -0.16]	0.001	0.097 [0.012, 0.207]	0.046	0.056 [-0.046, 0.151]	0.262
Posterior: Telophase	fixed	0.078 [0.04, 0.117]	0.002	-0.383 [-0.485, -0.283]	0.001	0.206 [0.101, 0.299]	0.001	0.048 [-0.051, 0.155]	0.344
Posterior: Cytokinesis	fixed	0.115 [0.079, 0.155]	0.001	-0.571 [-0.67, -0.479]	0.001	0.358 [0.242, 0.459]	0.001	0.025 [-0.09, 0.12]	0.618
Furrow Distance: Anaphase	fixed	-0.584 [-0.84, -0.332]	0.001	0.269 [-0.188, 0.798]	0.316	-2.146 [-2.792, -1.516]	0.001	-1.413 [-2.066, -0.857]	0.001
Furrow Distance: Telophase	fixed	-1.283 [-1.52, -1.053]	0.001	0.331 [-0.137, 0.837]	0.174	-3.031 [-3.567, -2.397]	0.001	-4.118 [-4.753, -3.45]	0.001
Furrow Distance: Cytokinesis	fixed	-2.305 [-2.521, -2.06]	0.001	0.44 [-0.007, 0.856]	0.054	-3.609 [-4.295, -3.053]	0.001	-5.817 [-6.424, -5.145]	0.001
Cell	random	0.044 [0.009, 0.107]	NA	0.735 [0.173, 1.677]	NA	0.272 [0.047, 0.705]	NA	0.657 [0.054, 1.807]	NA
units	residual	0.052 [0.05, 0.055]	NA	0.247 [0.235, 0.258]	NA	0.159 [0.149, 0.167]	NA	0.161 [0.15, 0.171]	NA

The estimated coefficients with 95% confidence interval from the MCMC GLMM models of the distribution of tagged NMY-2, TOE-2 and PIG-1, as well as the pMCMC value.

Table S2.2. RNAi of *nmy-2*

Genotype	Treatment	QL.a Defect	QL.p Defect
wild type	***nmy-2* RNAi**	9% N=34	12% N=34
nmy-2(ne1490)	**L4440**	0% N=100	3% N=100
nmy-2(ne1490)	***nmy-2* RNAi**	1% N=67	1% N=67
nmy-2(ne3409)	**L4440**	1% N=101	2% N=101
nmy-2(ne3409)	***nmy-2* RNAi**	16% N=134	7% N=134
nmy-2(ne3409); toe-2	**L4440**	29% N=55	35% N=55
nmy-2(ne3409); toe-2	***nmy-2* RNAi**	24% N=55	58% N=55
toe-2(gm408ok2807)	**L4440**	10% N=81	23% N=81
toe-2(gm408ok2807)	***nmy-2* RNAi**	21% N=72	40% N=72

Cell fate defects in worms grown at 25^{O}C on *nmy-2* RNAi or L4440 control bacteria. All strains contain the *gmIs81* transgene. Cell counts and filtering were performed as described in Figs 4-6.

Table S2.3. Mitotic potential in pig-1, toe-2, and temperature sensitive nmy-2 mutants

Genotype	# QL.pp Survived and divided	Total Surviving QL.pp	Frequency of QL.pp Division
pig-1(gm301)	79	171	46%
pig-1(gm344)	154	265	58%
toe-2(gm408ok2807)	8	50	16%
toe-2; pig-1(gm344)	85	236	36%
nmy-2(ne1490ts); pig-1(gm301)	180	282	64%
nmy-2(ne3409ts); pig-1(gm301)	96	169	57%
nmy-2(ne1490ts); toe-2	24	98	24%
nmy-2(ne3409ts); toe-2	16	65	25%

Cell counts with extra QL.pp daughter cells were divided between those in which the QL.pp daughter survived but did not divide, resulting in either 2 SDQLs or 2 PVMs and those where the QL.pp daughter survived and divided, resulting in 2 of both cell types. This determination of QL.pp mitotic potential makes the assumption that when there is an extra SDQL or PVM, the extra cell results from a QL.pp surviving and adopting the SDQL or PVM fate and that when there is both an extra SDQL and a PVM, the extra cells result from a QL.pp surviving and dividing to produce an SDQL and PVM

References

Arur, S., Ohmachi, M., Nayak, S., Hayes, M., Miranda, A., Hay, A., Golden, A., & Schedl, T. (2009). Multiple ERK substrates execute single biological processes in Caenorhabditis elegans germ-line development. *Proceedings of the National Academy of Sciences of the United States of America*, *106*(12), 4776–4781. https://doi.org/10.1073/pnas.0812285106

Barros, C. S., Phelps, C. B., & Brand, A. H. (2003). Drosophila nonmuscle myosin II promotes the asymmetric segregation of cell fate determinants by cortical exclusion rather than active transport. *Developmental Cell*, *5*(6), 829–840. https://doi.org/10.1016/S1534-5807(03)00359-9

Basant, A., & Glotzer, M. (2017). A GAP that Divides. *F1000Research*, *6*, 1788. https://doi.org/10.12688/f1000research.12064.1

Basant, A., Lekomtsev, S., Tse, Y. C., Zhang, D., Longhini, K. M., Petronczki, M., & Glotzer, M. (2015). Aurora B Kinase Promotes Cytokinesis by Inducing Centralspindlin Oligomers that Associate with the Plasma Membrane. *Developmental Cell*, *33*(2), 204–215. https://doi.org/10.1016/j.devcel.2015.03.015

Beaudet, D., Akhshi, T., Phillipp, J., Law, C., & Piekny, A. (2017). Active Ran regulates anillin function during cytokinesis. *Molecular Biology of the Cell*, *28*(24), 3517–3531. https://doi.org/10.1091/mbc.E17-04-0253

Brenner, S. (1974). The Genetics of Caenorhabditis elegans. *Genetics*, *77*(1), 71–94. https://doi.org/10.1093/genetics/77.1.71

Bringmann, H., Cowan, C. R., Kong, J., & Hyman, A. A. (2007). LET-99, GOA-1/GPA-16, and GPR-1/2 Are Required for Aster-Positioned Cytokinesis. *Current Biology*, *17*(2), 185–191. https://doi.org/10.1016/j.cub.2006.11.070

Bringmann, H., & Hyman, A. A. (2005). A cytokinesis furrow is positioned by two consecutive signals. *Nature*, *436*(7051), 731–734. https://doi.org/10.1038/nature03823

Cabernard, C., Prehoda, K. E., & Doe, C. Q. (2010). A spindle-independent cleavage furrow positioning pathway. *Nature*, *467*(7311), 91–94. https://doi.org/10.1038/nature09334

Chai, Y., Tian, D., Zhu, Z., Jiang, Y., Huang, S., Wu, D., Ou, G., & Li, W. (2022). Wnt signaling polarizes cortical actin polymerization to increase daughter cell asymmetry. *Cell Discovery*, *8*(1). https://doi.org/10.1038/s41421-022-00376-4

Chakraborty, S., Lambie, E. J., Bindu, S., Mikeladze-Dvali, T., & Conradt, B. (2015). Engulfment pathways promote programmed cell death by enhancing the unequal segregation of apoptotic potential. *Nature Communications*, *6*, 1–9. https://doi.org/10.1038/ncomms10126

Chapa-Y-Lazo, B., Hamanaka, M., Wray, A., Balasubramanian, M. K., & Mishima, M. (2020). Polar relaxation by dynein-mediated removal of cortical myosin II. *Journal of Cell Biology*, *219*(8). https://doi.org/10.1083/jcb.201903080

Chien, S. C., Brinkmann, E. M., Teuliere, J., & Garriga, G. (2013). Caenorhabditis elegans PIG-1/MELK acts in a conserved PAR-4/LKB1 polarity pathway to promote asymmetric neuroblast divisions. *Genetics*, *193*(3), 897–909. https://doi.org/10.1534/genetics.112.148106

Coffman, V. C., Kachur, T. M., Pilgrim, D. B., & Dawes, A. T. (2016). Antagonistic Behaviors of NMY-1 and NMY-2 Maintain Ring Channels in the C. elegans Gonad. *Biophysical Journal*, *111*(10), 2202–2213. https://doi.org/10.1016/j.bpj.2016.10.011

Connell, M., Cabernard, C., Ricketson, D., Doe, C. Q., & Prehoda, K. E. (2011). Asymmetric cortical extension shifts cleavage furrow position in Drosophila neuroblasts. *Molecular Biology of the Cell*, *22*(22), 4220–4226. https://doi.org/10.1091/mbc.E11-02-0173

Cordes, S., Frank, C. A., & Garriga, G. (2006). The C. elegans MELK ortholog PIG-1 regulates cell size asymmetry and daughter cell fate in asymmetric neuroblast divisions. *Development*, *133*(14), 2747–2756. https://doi.org/10.1242/dev.02447

Couwenbergs, C., Labbé, J. C., Goulding, M., Marty, T., Bowerman, B., & Gotta, M. (2007). Heterotrimeric G protein signaling functions with dynein to promote spindle positioning in C. elegans. *Journal of Cell Biology*, *179*(1), 15–22. https://doi.org/10.1083/jcb.200707085

Cowan, C. R., & Cowan, A. A. (2004). Centrosomes direct cell polarity independently of microtubule assembly in C. elegans embryos. *Nature*, *431*(7004), 92–96. https://doi.org/10.1038/nature02825

Dechant, R., & Glotzer, M. (2003). Centrosome separation and central spindle assembly act in redundant pathways that regulate microtubule density and trigger cleavage furrow formation. *Developmental Cell*, *4*(3), 333–344. https://doi.org/10.1016/S1534-5807(03)00057-1

Denning, D. P., Hatch, V., & Robert Horvitz, H. (2012). Programmed elimination of cells by caspase-independent cell extrusion in C. elegans. *Nature*, *488*(7410), 226–230. https://doi.org/10.1038/nature11240

Desai, C., Garriga, G., McIntire, S., & Horvitz, H. (1988). A genetic pathway for the development of the Caenorhabditis elegans HSN motor neurons. *Nature*, *336*, 638–646. http://www.wormbase.org/db/misc/paper?name=WBPaper00001105

Dickinson, D. J., Ward, J. D., Reiner, D. J., & Goldstein, B. (2013). Engineering the Caenorhabditis elegans genome using Cas9-triggered homologous recombination. *Nature Methods*, *10*(10), 1028–1034. https://doi.org/10.1038/nmeth.2641

Feng, G., Yi, P., Yang, Y., Chai, Y., Tian, D., Zhu, Z., Liu, J., Zhou, F., Cheng, Z., Wang, X., Li, W., & Ou, G. (2013). Developmental stage-dependent transcriptional regulatory pathways control neuroblast lineage progression. *Development (Cambridge)*, *140*(18), 3838–3847. https://doi.org/10.1242/dev.098723

Frank, C. A., Hawkins, N. C., Guenther, C., Horvitz, H. R., & Garriga, G. (2005). C. elegans HAM-1 positions the cleavage plane and regulates apoptosis in asymmetric neuroblast divisions. *Developmental Biology*, *284*(2), 301–310. https://doi.org/10.1016/j.ydbio.2005.05.026

Gallaud, E., Pham, T., & Cabernard, C. (2017). Drosophila melanogaster neuroblasts: A model for asymmetric stem cell divisions. In *Results and Problems in Cell Differentiation* (Vol. 61, pp. 183–210). https://doi.org/10.1007/978-3-319-53150-2_8

Galli, M., Muñoz, J., Portegijs, V., Boxem, M., Grill, S. W., Heck, A. J. R., & Van Den Heuvel, S. (2011). APKC phosphorylates NuMA-related LIN-5 to position the mitotic spindle during asymmetric division. *Nature Cell Biology*, *13*(9), 1132–1140. https://doi.org/10.1038/ncb2315

Ganguly, R., Mohyeldin, A., Thiel, J., Kornblum, H. I., Beullens, M., & Nakano, I. (2015). MELK—a conserved kinase: functions, signaling, cancer, and controversy. *Clinical and Translational Medicine*, *4*(1). https://doi.org/10.1186/s40169-014-0045-y

Gibrat, J. F., Madej, T., & Bryant, S. H. (1996). Surprising similarities in structure comparison. *Current Opinion in Structural Biology*, *6*(3), 377–385. https://doi.org/10.1016/S0959-440X(96)80058-3

Gotta, M., Dong, Y., Peterson, Y. K., Lanier, S. M., & Ahringer, J. (2003). Asymmetrically distributed C. elegans Homologs of AGS3/PINS control spindle position in the early embryo. *Current Biology*, *13*(12), 1029–1037. https://doi.org/10.1016/S0960-9822(03)00371-3

Goupil, E., Amini, R., Hall, D. H., & Labbé, J. C. (2017). Actomyosin contractility regulators stabilize the cytoplasmic bridge between the two primordial germ cells during Caenorhabditis elegans embryogenesis. *Molecular Biology of the Cell*, *28*(26), 3789–3800. https://doi.org/10.1091/mbc.E17-08-0502

Guenther, C., & Garriga, G. (1996). Asymmetric distribution of the C. elegans HAM-1 protein in neuroblasts enables daughter cells to adopt distinct fates. *Development*, *122*(11), 3509–3518. https://doi.org/10.1242/dev.122.11.3509

Guo, S., & Kemphues, K. J. (1996). A non-muscle myosin required for embryonic polarity in Caenorhabditis elegans. *Nature*, *382*(6590), 455–458. https://doi.org/10.1038/382455a0

Gurling, M., Talavera, K., & Garriga, G. (2014). The DEP domain-containing protein TOE-2 promotes apoptosis in the Q lineage of C. Elegans through two distinct mechanisms. *Development (Cambridge)*, *141*(13), 2724–2734. https://doi.org/10.1242/dev.110486

Hadfield, J. D. (2010). MCMCglmm: MCMC Methods for Multi-Response GLMMs in R. *Journal of Statistical Software*, *33*(2), 1–22. http://www.jstatsoft.org/

Hird, S. N., & White, J. G. (1993). Cortical and cytoplasmic flow polarity in early embryonic cells of Caenorhabditis elegans. *Journal of Cell Biology*, *121*(6), 1343–1355. https://doi.org/10.1083/jcb.121.6.1343

Horvitz, H. R., & Herskowitz, I. (1992). Mechanisms of asymmetric cell division: Two Bs or not two Bs, that is the question. *Cell*, *68*(2), 237–255. https://doi.org/10.1016/0092-8674(92)90468-R

Jantsch-Plunger, V., Gönczy, P., Romano, A., Schnabel, H., Hamill, D., Schnabel, R., Hyman, A. A., & Glotzer, M. (2000). CYK-4: A Rho family GTPase activating protein (GAP) required for central spindle formation and cytokinesis. *Journal of Cell Biology*, *149*(7), 1391–1404. https://doi.org/10.1083/jcb.149.7.1391

Jumper, J., Evans, R., Pritzel, A., Green, T., Figurnov, M., Ronneberger, O., Tunyasuvunakool, K., Bates, R., Žídek, A., Potapenko, A., Bridgland, A., Meyer, C., Kohl, S. A. A., Ballard, A. J., Cowie, A., Romera-Paredes, B., Nikolov, S., Jain, R., Adler, J., … Hassabis, D. (2021). Highly accurate protein structure prediction with AlphaFold. *Nature*, *596*(7873), 583–589. https://doi.org/10.1038/s41586-021-03819-2

Kamath, R. S., & Ahringer, J. (2003). Genome-wide RNAi screening in Caenorhabditis elegans. *Methods*, *30*(4), 313–321. https://doi.org/10.1016/S1046-2023(03)00050-1

Krueger, L. E., Wu, J. C., Tsou, M. F. B., & Rose, L. S. (2010). LET-99 inhibits lateral posterior pulling forces during asymmetric spindle elongation in C. elegans embryos. *Journal of Cell Biology*, *189*(3), 481–495. https://doi.org/10.1083/jcb.201001115

Lenth, R. (2019). Emmeans: estimated marginal means. In *R package version 1.4.2* (p. https://cran.r-project.org/package=emmeans). https://github.com/rvlenth/emmeans%0Ahttps://cran.r-project.org/package=emmeans

Leung, A., Hua, K., Ramachandran, P., Hingwing, K., Wu, M., Koh, P. L., & Hawkins, N. (2016). C. elegans HAM-1 functions in the nucleus to regulate asymmetric neuroblast division. *Developmental Biology*, *410*(1), 56–69. https://doi.org/10.1016/j.ydbio.2015.12.011

Liro, M. J., Morton, D. G., & Rose, L. S. (2018). The kinases PIG-1 and PAR-1 act in redundant pathways to regulate asymmetric division in the EMS blastomere of C. elegans. *Developmental Biology*, *444*(1), 9–19. https://doi.org/10.1016/j.ydbio.2018.08.016

Liro, M. J., & Rose, L. S. (2016). Mitotic spindle positioning in the EMS cell of Caenorhabditis elegans requires LET-99 and LIN-5/NuMA. *Genetics*, *204*(3), 1177–1189. https://doi.org/10.1534/genetics.116.192831

Liu, J., Maduzia, L. L., Shirayama, M., & Mello, C. C. (2010). NMY-2 maintains cellular asymmetry

and cell boundaries, and promotes a SRC-dependent asymmetric cell division. *Developmental Biology*, *339*(2), 366–373. https://doi.org/10.1016/j.ydbio.2009.12.041

Lizcano, J. M., Göransson, O., Toth, R., Deak, M., Morrice, N. A., Boudeau, J., Hawley, S. A., Udd, L., Mäkelä, T. P., Hardie, D. G., & Alessi, D. R. (2004). LKB1 is a master kinase that activates 13 kinases of the AMPK subfamily, including MARK/PAR-1. *EMBO Journal*, *23*(4), 833–843. https://doi.org/10.1038/sj.emboj.7600110

Mishima, M., Kaitna, S., & Glotzer, M. (2002). Central spindle assembly and cytokinesis require a kinesin-like protein/RhoGAP complex with microtubule bundling activity. *Developmental Cell*, *2*(1), 41–54. https://doi.org/10.1016/S1534-5807(01)00110-1

Mishima, M., Pavicic, V., Grüneberg, U., Nigg, E. A., & Glotzer, M. (2004). Cell cycle regulation of central spindle assembly. *Nature*, *430*(7002), 908–913. https://doi.org/10.1038/nature02767

Mishra, N., Wei, H., & Conradt, B. (2018). Caenorhabditis elegans ced-3 caspase is required for asymmetric divisions that generate cells programmed to die. *Genetics*, *210*(3), 983–998. https://doi.org/10.1534/genetics.118.301500

Morita, K., Hirono, K., & Han, M. (2005). The Caenorhabditis elegans ect-2 RhoGEF gene regulates cytokinesis and migration of epidermal P cells. *EMBO Reports*, *6*(12), 1163–1168. https://doi.org/10.1038/sj.embor.7400533

Motegi, F., & Sugimoto, A. (2006). Sequential functioning of the ECT-2 RhoGEF, RHO-1 and CDC-42 establishes cell polarity in Caenorhabditis elegans embryos. *Nature Cell Biology*, *8*(9), 978–985. https://doi.org/10.1038/ncb1459

Munro, E., Nance, J., & Priess, J. R. (2004). Cortical flows powered by asymmetrical contraction transport PAR proteins to establish and maintain anterior-posterior polarity in the early C. elegans embryo. *Developmental Cell*, *7*(3), 413–424. https://doi.org/10.1016/j.devcel.2004.08.001

Nance, J., Munro, E. M., & Priess, J. R. (2003). C. elegans PAR-3 and PAR-6 are required for apicobasal asymmetries associated with cell adhesion and gastrulation. *Development*, *130*(22), 5339–5350. https://doi.org/10.1242/dev.00735

Nguyen-Ngoc, T., Afshar, K., & Gönczy, P. (2007). Coupling of cortical dynein and Gα proteins mediates spindle positioning in Caenorhabditis elegans. *Nature Cell Biology*, *9*(11), 1294–1302. https://doi.org/10.1038/ncb1649

Ou, G., Stuurman, N., D'Ambrosio, M., & Vale, R. D. (2010). Polarized myosin produces unequal-size daughters during asymmetric cell division. *Science*, *330*(6004), 677–680. https://doi.org/10.1126/science.1196112

Pacquelet, A. (2017). Asymmetric cell division in the one-cell C. Elegans embryo: Multiple steps

to generate cell size asymmetry. In J.-P. Tassan & J. Z. Kubiak (Eds.), *Results and Problems in Cell Differentiation* (Vol. 61, pp. 115–140). Springer International Publishing. https://doi.org/10.1007/978-3-319-53150-2_5

Pacquelet, A., Uhart, P., Tassan, J. P., & Michaux, G. (2015). PAR-4 and anillin regulate myosin to coordinate spindle and furrow position during asymmetric division. *Journal of Cell Biology*, *210*(7), 1085–1099. https://doi.org/10.1083/jcb.201503006

Park, D. H., & Rose, L. S. (2008). Dynamic localization of LIN-5 and GPR-1/2 to cortical force generation domains during spindle positioning. *Developmental Biology*, *315*(1), 42–54. https://doi.org/10.1016/j.ydbio.2007.11.037

Piekny, A. J., & Glotzer, M. (2008). Anillin Is a Scaffold Protein That Links RhoA, Actin, and Myosin during Cytokinesis. *Current Biology*, *18*(1), 30–36. https://doi.org/10.1016/j.cub.2007.11.068

Raich, W. B., Moran, A. N., Rothman, J. H., & Hardin, J. (1998). Cytokinesis and midzone microtubule organization in Caenorhabditis elegans require the kinesin-like protein ZEN-4. *Molecular Biology of the Cell*, *9*(8), 2037–2049. https://doi.org/10.1091/mbc.9.8.2037

Robinson, J., Teuliere, J., Yoo, S., & Garriga, G. (2022). NMY-2, TOE-2 and PIG-1 Regulate C. elegans Asymmetric Cell Divisions. *BioRxiv*, 2022.11.17.516947. https://doi.org/10.1101/2022.11.17.516947

Sadler, P. L., & Shakes, D. C. (2000). Anucleate Caenorhabditis elegans sperm can crawl, fertilize oocytes and direct anterior-posterior polarization of the I-cell embryo. *Development*, *127*(2), 355–366. https://doi.org/10.1242/dev.127.2.355

Schindelin, J., Arganda-Carreras, I., Frise, E., Kaynig, V., Longair, M., Pietzsch, T., Preibisch, S., Rueden, C., Saalfeld, S., Schmid, B., Tinevez, J. Y., White, D. J., Hartenstein, V., Eliceiri, K., Tomancak, P., & Cardona, A. (2012). Fiji: An open-source platform for biological-image analysis. *Nature Methods*, *9*(7), 676–682. https://doi.org/10.1038/nmeth.2019

Siller, K. H., Cabernard, C., & Doe, C. Q. (2006). The NuMA-related Mud protein binds Pins and regulates spindle orientation in Drosophila neuroblasts. *Nature Cell Biology*, *8*(6), 594–600. https://doi.org/10.1038/ncb1412

Sulston, J. E., & Horvitz, H. R. (1977). Post-embryonic cell lineages of the nematode, Caenorhabditis elegans. *Developmental Biology*, *56*(1), 110–156. https://doi.org/10.1016/0012-1606(77)90158-0

Sulston, J. E., Schierenberg, E., White, J. G., & Thomson, J. N. (1983). The embryonic cell lineage of the nematode Caenorhabditis elegans. *Developmental Biology*, *100*(1), 64–119. https://doi.org/10.1016/0012-1606(83)90201-4

Teuliere, J., Cordes, S., Singhvi, A., Talavera, K., & Garriga, G. (2014). Asymmetric neuroblast

divisions producing apoptotic cells require the cytohesin GRP-1 in caenorhabditis elegans. *Genetics*, *198*(1), 229–247. https://doi.org/10.1534/genetics.114.167189

Teuliere, J., & Garriga, G. (2017). Size Matters: How C. elegans Asymmetric Divisions Regulate Apoptosis. In J.-P. Tassan & J. Z. Kubiak (Eds.), *Asymmetric Cell Division in Development, Differentiation and Cancer* (pp. 141–163). Springer International Publishing. https://doi.org/10.1007/978-3-319-53150-2_6

Teuliere, J., & Garriga, G. (2018). The Caenorhabditis elegans HAM-1 protein modifies G protein signaling and membrane extension to reverse the polarity of asymmetric cell division. *BioRxiv*. https://doi.org/10.1101/504787

Teuliere, J., Kovacevic, I., Bao, Z., & Garriga, G. (2018). The Caenorhabditis elegans gene ham-1 regulates daughter cell size asymmetry primarily in divisions that produce a small anterior daughter cell. *PLoS ONE*, *13*(4), 1–14. https://doi.org/10.1371/journal.pone.0195855

Tsankova, A., Pham, T. T., Garcia, D. S., Otte, F., & Cabernard, C. (2017). Cell Polarity Regulates Biased Myosin Activity and Dynamics during Asymmetric Cell Division via Drosophila Rho Kinase and Protein Kinase N. *Developmental Cell*, *42*(2), 143-155.e5. https://doi.org/10.1016/j.devcel.2017.06.012

Tse, Y. C., Piekny, A., & Glotzera, M. (2011). Anillin promotes astral microtubule-directed cortical myosin polarization. *Molecular Biology of the Cell*, *22*(17), 3165–3175. https://doi.org/10.1091/mbc.E11-05-0399

Tse, Y. C., Werner, M., Longhini, K. M., Labbe, J. C., Goldstein, B., & Glotzer, M. (2012). RhoA activation during polarization and cytokinesis of the early Caenorhabditis elegans embryo is differentially dependent on NOP-1 and CYK-4. *Molecular Biology of the Cell*, *23*(20), 4020–4031. https://doi.org/10.1091/mbc.E12-04-0268

Tsou, M. F. B., Hayashi, A., DeBella, L. R., McGrath, G., & Rose, L. S. (2002). LET-99 determines spindle position and is asymmetrically enriched in response to PAR polarity cues in C. elegans embryos. *Development*, *129*(19), 4469–4481. https://doi.org/10.1242/dev.129.19.4469

Varadi, M., Anyango, S., Deshpande, M., Nair, S., Natassia, C., Yordanova, G., Yuan, D., Stroe, O., Wood, G., Laydon, A., Zídek, A., Green, T., Tunyasuvunakool, K., Petersen, S., Jumper, J., Clancy, E., Green, R., Vora, A., Lutfi, M., … Velankar, S. (2022). AlphaFold Protein Structure Database: Massively expanding the structural coverage of protein-sequence space with high-accuracy models. *Nucleic Acids Research*, *50*(D1), D439–D444. https://doi.org/10.1093/nar/gkab1061

Wang, Y., Lee, Y. M., Baitsch, L., Huang, A., Xiang, Y., Tong, H., Lako, A., Von, T., Choi, C., Lim, E., Min, J., Li, L., Stegmeier, F., Schlegel, R., Eck, M. J., Gray, N. S., Mitchison, T. J., & Zhao, J. J. (2014). MELK is an oncogenic kinase essential for mitotic progression in basal-like breast

cancer cells. *ELife*, *2014*(3), 1–27. https://doi.org/10.7554/eLife.01763

Wei, H., Lambie, E. J., Osório, D. S., Carvalho, A. X., & Conradt, B. (2020). PIG-1 MELK-dependent phosphorylation of nonmuscle myosin II promotes apoptosis through CES-1 Snail partitioning. *PLoS Genetics*, *16*(9), 1–27. https://doi.org/10.1371/journal.pgen.1008912

Wei, H., Yan, B., Gagneur, J., & Conradt, B. (2017). Caenorhabditis elegans CES-1 snail represses Pig-1 MELK expression to control asymmetric cell division. *Genetics*, *206*(4), 2069–2084. https://doi.org/10.1534/genetics.117.202754

Werner, M., Munro, E., & Glotzer, M. (2007). Astral Signals Spatially Bias Cortical Myosin Recruitment to Break Symmetry and Promote Cytokinesis. *Current Biology*, *17*(15), 1286–1297. https://doi.org/10.1016/j.cub.2007.06.070

Wickham, H. (2010). ggplot2: Elegant Graphics for Data Analysis. In *Journal of Statistical Software* (Vol. 35, Issue Book Review 1). Springer-Verlag New York. https://doi.org/10.18637/jss.v035.b01

Wickham, H. (2014). Tidy Data. *Journal of Statistical Software*, *59*(10), 1–23. http://www.jstatsoft.org/

Wu, J.-C., Espiritu, E. B., & Rose, L. S. (2016). The 14-3-3 protein PAR-5 regulates the asymmetric localization of the LET-99 spindle positioning protein. *Developmental Biology*, *412*(2), 288–297. https://doi.org/10.1016/j.ydbio.2016.02.020

Wu, J.-C., & Rose, L. S. (2007). PAR-3 and PAR-1 Inhibit LET-99 Localization to Generate a Cortical Band Important for Spindle Positioning in Caenorhabditis elegans Embryos. *Molecular Biology of the Cell*, *18*(11), 4470–4482. https://doi.org/10.1091/mbc.e07-02-0105

Zhang, D., & Glotzer, M. (2015). The RhoGAP activity of CYK-4/MgcRacGAP functions non-canonically by promoting RhoA activation during cytokinesis. *ELife*, *4*(AUGUST2015), 1–25. https://doi.org/10.7554/eLife.08898

Zhu, Z., Liu, J., Yi, P., Tian, D., Chai, Y., Li, W., & Ou, G. (2014). A proneural gene controls C. elegans neuroblast asymmetric division and migration. *FEBS Letters*, *588*(7), 1136–1143. https://doi.org/10.1016/j.febslet.2014.02.036

Zonies, S., Motegi, F., Hao, Y., & Seydoux, G. (2010). Symmetry breaking and polarization of the C. elegans zygote by the polarity protein PAR-2. *Development*, *137*(10), 1669–1677. https://doi.org/10.1242/dev.045823

Appendix A: Genetic interaction between *toe-2* and *pig-1* in Q lineage DCSA

A.1 Introduction

In our experiments we investigated the interactions between *nmy-2* and *toe-2* as well as *nmy-2* and *pig-1* and observed the impacts on DCSA and cell fate determination of these mutations. To further characterize the relationship between these regulators we performed the same experiments with double mutants of *toe-2* and *pig-1*.

A.2 Results

We constructed *toe-2(gm408ok2807); pig-1(gm344)* double mutants and analyzed the fates of their descendants (Fig A.1). The *toe-2(gm408ok2807)* mutation suppresses the *pig-1(gm344)* defects in Q lineage cell fate, while simultaneously increasing the frequency of missing cells. When cell fate transformations are excluded as before, there is a significant decrease in frequency of QL.p defects in the double mutant compared to *pig-1(gm344)* alone. However, only in QL.a is it reduced to the same level as *toe-2(gm408ok2807)*.

A portion of the reduced frequency of extra Q.p cells, particularly SDQLs, can be explained by a reduction in mitotic potential. There was a significant decrease in the frequency of Q.pp divisions in *toe-2(gm408ok2807); pig-1(gm344)* compared to *pig-1(gm344)* (36%, N=321 vs 58%, N=419, $p<0.001$) (Table S2.3). However, this was also significantly greater than the frequency of Q.pp divisions in *toe-2(gm408ok2807)* on its own (16%, N=58, $p<0.01$).

There was a significant, $p<0.001$, increase in the frequency of missing PQRs for *toe-2; pig-1* compared to *toe-2.* There is no significant increase in the frequency of other missing cells. The largest part of the increase in missing PQRs comes from a significant ($p<0.01$) increase in frequency of worms missing all QL markers.

Unfortunately, we were not able to perform reliable DCSA measurements with strains containing *toe-2(gm408ok2807)* and either *pig-1(gm280)*, a previously characterized hypomorph, or *pig-1(gm344)*. This was due to a combination of ectopic expression of the *Pegl-17::GFP* marker in the L1 stage, severe defects in cell migration, and the general ill-health of the larvae.

A.3 Conclusion

We observed a suppression of *pig-1(gm344)* QL.a defects in *toe-2(gm408ok2807); pig-1(gm344)*, suggesting that *toe-2* is downstream of PIG-1 in the QL.a division. We also observed a partial suppression of *pig-1(gm344)* QL.p defects in *toe-2(gm408ok2807); pig-1(gm344)*, as well as a partial reduction of QL.pp mitotic potential. This implies that TOE-2 may be a downstream effector of PIG-1 and some of PIG-1's phenotype is produced by inappropriate activity of TOE-2.

Supporting evidence that there is an interaction between TOE-2 and PIG-1 is the disruption independent of Q lineage DCSA. While we do not know their precise origin, we observed severe defects in fertility and growth, ectopic expression of the *egl-17* promoter, and the loss and duplication of the Q neuroblast lineage, all of which suggest that there was an increase in cell fate determination defects in other cells during development.

A.4 Figure

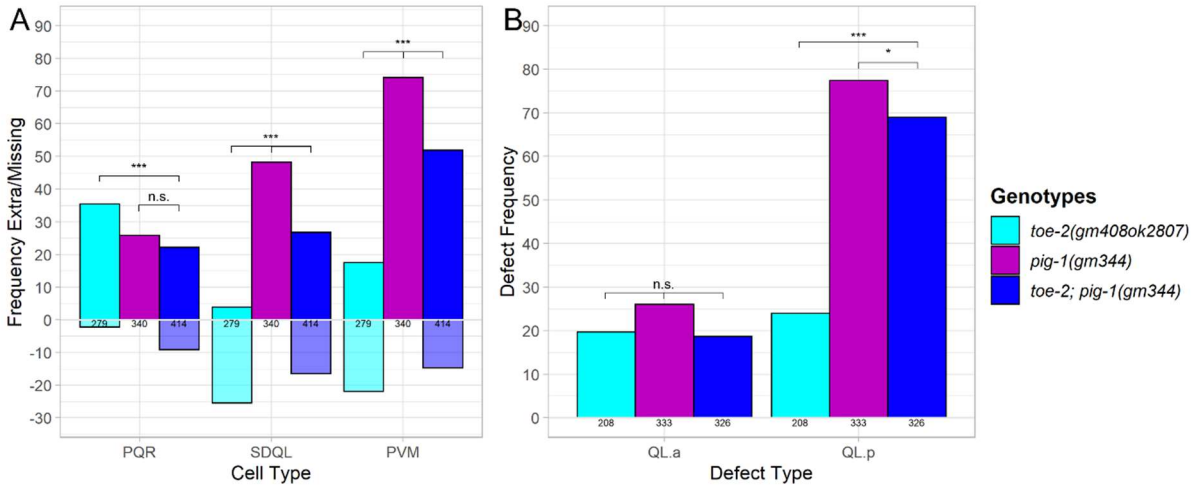

Fig A.1. The double mutant *toe-2; pig-1* has an intermediate phenotype.
A) Frequency of extra (positive y axis) and missing (negative y axis) QL lineage cells in worms with *toe-2(gm408ok2807), pig-1(gm344)*, or the *toe-2(gm408ok2807); pig-1(gm344)* genotypes. B) Frequency of defects that originate specifically from the QL.p and QL.a divisions. *: P<0.05, **: P<0.01, ***: P<0.001, n.s.: P>0.05.

Appendix B: The role of *ect-2* in Q lineage DCSA

B.1 Introduction

NMY-2 is known to be regulated by Rho in the asymmetric first cell division, while Rho activity is regulated by the Rho-GAP ECT-2. To determine if NMY-2 acts in the same pathway as ECT-2 in the Q lineage, we tested the impact of the temperature-sensitive *ect-2(ax751ts)* on Q lineage DCSA as well as double mutants with *ect-2(ax751ts)* and the temperature sensitive *nmy-2(ne1490ts)* allele.

B.2 Results

The *ect-2(ax751ts)* mutation resulted in very similar phenotypes as the *nmy-2(ne1490ts)* allele, with a significant, though slight, loss of asymmetry in the Q.p division (Fig B.1B) but not in Q.a (Fig B.1A). This strain also had significant increases in the frequency of extra Q lineage cells (Fig B.1C,D).

Consistent with the two genes acting together in asymmetric cell division, there were no significant DCSA differences between the *nmy-2* and *ect-2* single mutants and the *nmy-2(ne1490ts); ect-2(ax751ts)* double mutant (Fig B.1 A,B). Similarly, there was no significant difference between the cell fate between the *ect-2(ax751)* single mutant and the double mutant for both QL.a and QL.p (Fig B.1C,D).

B.3 Conclusion

Because neither mutant alters Q.a DCSA, the lack of an enhancement is difficult to interpret, but because the mutants do alter Q.p DCSA, the lack of enhancement suggests that *nmy-2* and *ect-2* function together to regulate the size asymmetry of this division. The lack of a significant difference between the single and double mutants with respect to Q lineage cell fate defects further supports the hypothesis that they function together in the regulation of Q lineage cell fate.

B.4 Figure

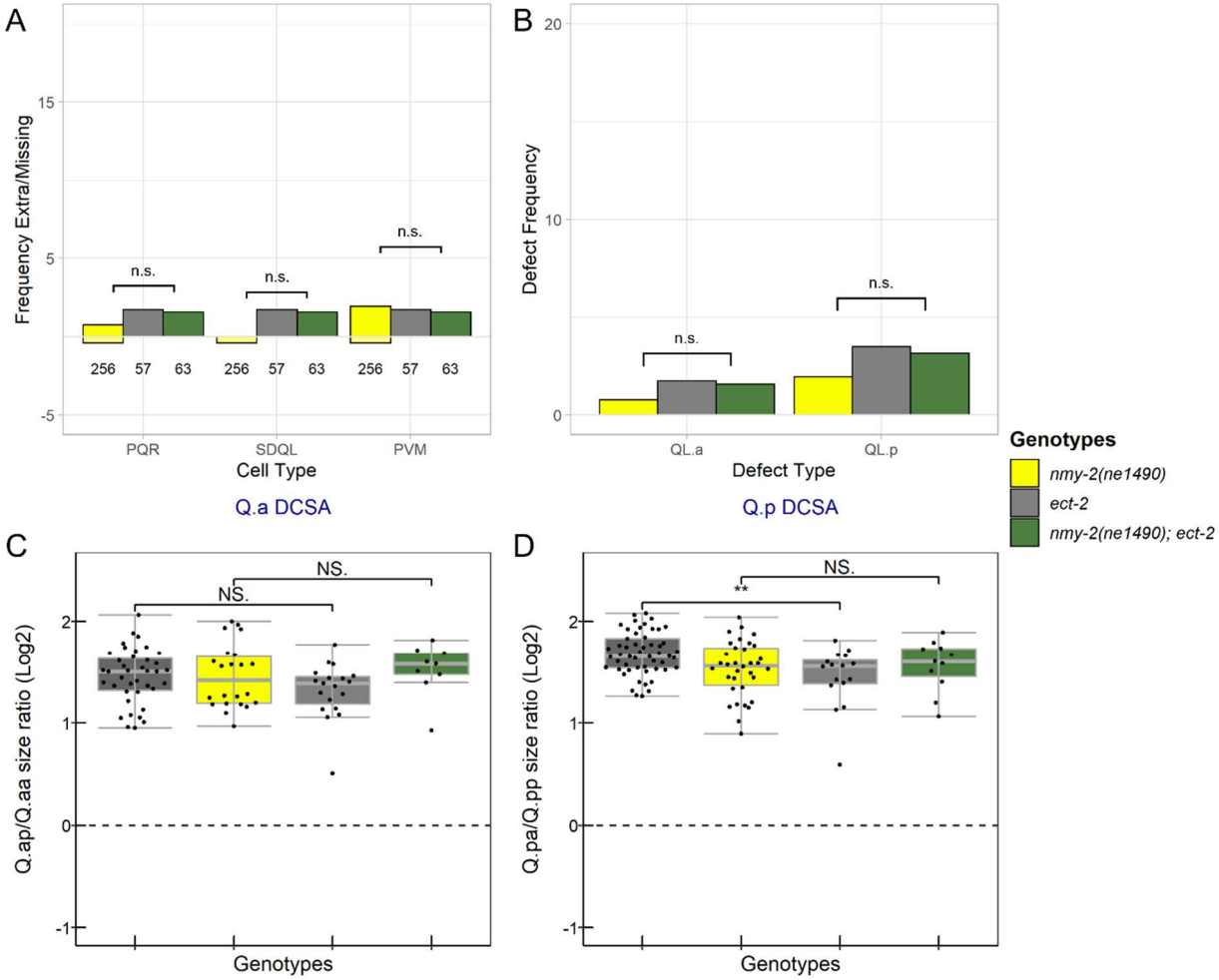

Fig B.1. DCSA and Q lineage cell-fate defects in temperature-sensitive *ect-2* and *nmy-2; ect-2* mutants.

A) Comparison of measured areas of A) Q.ap/Q.aa and B) Q.pa/Q.pp divisions in control, *ect-2*, *nmy-2(ne1490ts)* mutants, and the double mutant. C) Frequency of extra (positive y axis) and missing (negative y axis) QL lineage cells in *ect-2, nmy-2(ne1490*ts*)* mutants, and the double mutants D) Frequency of extra cell defects that could be explained by survival of QL.aa or QL.pp with no other cell fate transformations. Below each bar are the number of lineages scored. *: P<0.05, **: P<0.01, ***: P<0.001, n.s.: P>0.05.